Neurobiology of Disease

Accumulation of α-Synuclein Triggered by Presynaptic Dysfunction

Yasuto Nakata,[1,4] Toru Yasuda,[1,4,5] Masahiro Fukaya,[2] Saori Yamamori,[3] Makoto Itakura,[3] Tomoko Nihira,[1,4] Hideki Hayakawa,[1,4] Aya Kawanami,[1] Masakazu Kataoka,[6] Makiko Nagai,[1] Hiroyuki Sakagami,[2] Masami Takahashi,[3] Yoshikuni Mizuno,[4] and Hideki Mochizuki[1,4,5]

Departments of [1]Neurology, [2]Anatomy, and [3]Biochemistry, and [4]Division of Neuroregenerative Medicine, Kitasato University School of Medicine, Sagamihara, Kanagawa 252-0374, Japan, [5]Department of Neurology, Osaka University Graduate School of Medicine, Suita, Osaka 565-0871, Japan, and [6]Department of Environmental Science and Technology, Faculty of Engineering, Shinshu University, Nagano-shi, Nagano 380-8553, Japan

Pathological examination of dementia with Lewy bodies patients identified the presence of abnormal α-synuclein (αSyn) aggregates in the presynaptic terminals. αSyn is involved in the regulation of soluble *N*-ethylmaleimide-sensitive factor attachment protein receptor (SNARE) complex. Importantly, αSyn-transgenic mouse and postmortem examination of patients with Parkinson's disease have demonstrated the abnormal distribution of SNARE protein in presynaptic terminals. In this study, we investigated the effects of SNARE dysfunction on endogenous αSyn using *Snap25*$^{S187A/S187A}$ mutant mice. These mice have homozygous knock-in gene encoding unphosphorylatable S187A-substituted synaptosomal-associated protein of 25 kDa (SNAP-25). The mice displayed a significant age-dependent change in the distribution of αSyn and its Ser^{129}-phosphorylated form in abnormally hypertrophied glutamatergic nerve terminals in the striatum. Electron-microscopic analysis revealed the abnormally condensed synaptic vesicles with concomitant mislocalization of αSyn protein to the periactive zone in the glutamatergic nerve terminals. However, the *Snap25*$^{S187A/S187A}$ mutant mouse harbored no abnormalities in the nigrostriatal dopaminergic neurons. Our present results suggest that SNARE dysfunction is the initial trigger of mislocalization and accumulation of αSyn, and probably is an important pathomechanism of α-synucleinopathies.

Introduction

α-Synucleinopathies are a subgroup of neurodegenerative diseases including dementia with Lewy bodies (DLB), multiple system atrophy (MSA), and Parkinson's disease (PD). The pathological hallmark of the disorders is the formation of intracellular aggregates composed mainly of α-synuclein (αSyn), which are called Lewy bodies and Lewy neurites (Spillantini and Goedert, 2000; Galvin et al., 2001; Yasuda et al., 2012). It was reported recently that >90% of αSyn aggregates are present in presynaptic terminals in the form of very small deposits of the affected neurons in DLB (Neumann et al., 2002; Kramer and Schulz-Schaeffer, 2007; Schulz-Schaeffer, 2010). However, the mechanisms responsible for presynaptic accumulation of abnormal αSyn remain elusive.

Received May 8, 2012; revised Aug. 28, 2012; accepted Oct. 5, 2012.

Author contributions: Y.N., T.Y., and H.M. designed research; Y.N., T.Y., M.F., S.Y., M.I., T.N., H.H., and A.K. performed research; Y.N., T.Y., M.F., S.Y., M.I., T.N., H.H., A.K., M.K., M.N., H.S., M.T., Y.M., and H.M. analyzed data; Y.N. and T.Y. wrote the paper.

This work was supported by Grants from the Japan Science and Technology Agency, Core Research for Evolutional Science and Technology (H.M.); Grants-in-Aid from the Research Committee of CNS Degenerative Diseases, the Ministry of Health, Labour and Welfare of Japan (H.M.); Grant-in-Aid for Research on Applying Health Technology (H23–015) from the Ministry of Health, Labour and Welfare of Japan (H.M.); Ministry of Education, Culture, Sports, Science and Technology of Japan Grant S0801035 (H.M.); and Grant-in-Aid for Scientific Research on Innovative Areas (Brain Environment) from the Ministry of Education, Science, Sports and Culture of Japan (H.M.).

The authors declare no competing financial interests.

Correspondence should be addressed to Prof. Hideki Mochizuki, Department of Neurology, Osaka University Graduate School of Medicine, 2-2 Yamadaoka, Suita, Osaka 565-0871, Japan. E-mail: hmochizuki@neurol.med.osaka-u.ac.jp.

DOI:10.1523/JNEUROSCI.2220-12.2012

 0270-6474/12/3217186-11$15.00/0

Generally, αSyn is abundantly localized in the presynaptic nerve terminals (Maroteaux et al., 1988; Iwai et al., 1995). While the physiological functions of αSyn have yet to be defined, several lines of evidence implicated this protein in the modulation of neurotransmitter release through the regulation of formation of the soluble *N*-ethylmaleimide-sensitive factor attachment protein receptor (SNARE) complex (Chandra et al., 2005; Burré et al., 2010; Darios et al., 2010) and the size of synaptic vesicle pool (Murphy et al., 2000; Cabin et al., 2002; Larsen et al., 2006; Nemani et al., 2010). Vesicle-associated membrane protein-2 (VAMP-2) present in the synaptic vesicles, and syntaxin and synaptosomal-associated protein of 25 kDa (SNAP-25) in the presynaptic plasma membrane form the core SNARE complex, which regulate the docking and fusion of synaptic vesicles to the presynaptic membrane (Südhof, 2004). A recent study showed the physical interaction of αSyn with VAMP-2 to promote SNARE assembly (Burré et al., 2010). Cysteine-string protein-α (CSPα) also participates in SNARE assembly, and mutant mice lacking CSPα displayed impaired SNARE formation and premature death, but both of these phenotypes are counteracted by transgenic expression of αSyn (Chandra et al., 2005; Sharma et al., 2011). However, overexpression of αSyn with no overt toxicity inhibits neurotransmitter release, due to a defective reclustering of synaptic vesicles after endocytosis (Nemani et al., 2010). Additionally, overexpressed αSyn indirectly inhibited SNARE-mediated exocytosis by sequestering arachidonic acid, which upregulates syntaxin and enhances its engagement with SNARE complex (Darios et al., 2010). Importantly, abnormal redistribu-

tion of SNARE proteins has been observed in human PD patients and mice overexpressing a truncated form of human αSyn, which showed decreased release of dopamine (DA) in the striatum (Garcia-Reitböck et al., 2010). Therefore, presynaptic SNARE dysfunction is considered an initial pathogenic event in α-synucleinopathies.

Based on the above background, the present study was designed to investigate the effects of impaired SNARE assembly on the distribution of naive αSyn. We exploited *Snap25*$^{S187A/S187A}$ mutant mice. This strain is resistant to the protein kinase C-mediated phosphorylation of SNAP-25 at *Ser*^{187} and represents a concomitant reduction of neurotransmitter release, including serotonin and DA, from the amygdala, and develops convulsive seizures and anxiety-related behavior in general activity and light-and-dark preference tests (Kataoka et al., 2011). The results indicated that dysfunction of SNARE proteins could trigger abnormal localization and accumulation of presynaptic αSyn, possibly representing one of the pathogenic events in DLB or MSA.

Materials and Methods

Mice. All experimental protocols described in this study were approved by the Animal Experimentation and Ethics Committee of the Kitasato University School of Medicine. Homozygous SNAP-25 knock-in mutant mice bearing S187A mutation and wild-type littermate control mice were generated based on the procedures described in detail by Kataoka et al. (2011). Briefly, embryonic stem cells with the heterozygous *Snap25*^{S187A} mutant allele were generated and microinjected into C57BL/6N blastocysts to obtain heterozygous mutant mice. Male chimeras were bred with C57BL/6N female mice. After the line was backcrossed 13 times, homozygous mice (designated as *Snap25*$^{S187A/S187A}$ mice) were obtained by *in vitro* fertilization. The genotype was checked by PCR. In this experiment, wild-type and *Snap25*$^{S187A/S187A}$ mice were used at age 11 (females), 54 (females), 60 (males), and 61 (females) weeks.

Tissue processing. Deeply anesthetized mice (with 250 mg/kg, i.p., sodium pentobarbital) were perfused transcardially with PBS or with 2% paraformaldehyde/2% glutaraldehyde in 0.1 M phosphate buffer (PB). The brains were removed en bloc from the skull and cut sagittally into two brain hemispheres for confocal microscopy, cell counting, electron microscopy, Western blotting, and catecholamine analysis. Tissue processing for conventional electron microscopy is described below (see Conventional electron microscopy). For confocal microscopy and cell counting, hemisphere brain blocks of mice perfused transcardially with PBS or with 2% paraformaldehyde/2% glutaraldehyde in 0.1 M PB were fixed overnight in 4% paraformaldehyde in PBS and immersed in PBS containing 30% sucrose until sinking. Coronal sections of the striatum and the entire rostrocaudal extent of the substantia nigra (SN) were cut serially at 20 μm thickness using a cryostat (CM1850; Leica Microsystems). For Western blotting and catecholamine measurement by HPLC, brain blocks of mice perfused transcardially with PBS were dissected using the method described previously by our group, to yield the striatal tissues and ventral parts of midbrain tissues including the SN (Yasuda et al., 2011). After completing the dissection, the sections were immediately frozen on dry ice and stored at −80°C until analysis.

Antibodies. The primary antibodies used for confocal microscopy were mouse anti-αSyn (clone 42; diluted at 1:100; BD Biosciences) (Tapia-González et al., 2011), rabbit anti-αSyn (1:500; Millipore Bioscience Research Reagents) (Chung et al., 2003; Herzig et al., 2011), rabbit anti-tyrosine hydroxylase (TH) (1:5000; Calbiochem) (Yasuda et al., 2011), mouse anti-synaptophysin (clone SY38; 1:500; Millipore) (Masliah et al., 2001; Tabuchi et al., 2007; Gimbel et al., 2010), rat anti-dopamine transporter (DAT) (clone MAB369; 1:500; Millipore) (Herzig et al., 2011; Kaushal et al., 2011), rabbit or goat anti-vesicular glutamate transporter-1 (VGLUT1) (1:300; Frontier Institute) (Miyazaki et al., 2003; Kawamura et al., 2006), goat anti-VGLUT2 (1:300; Frontier Institute) (Miyazaki et al., 2003; Kawamura et al., 2006), and rabbit anti-Ser^{129}-phosphorylated αSyn (ab59264; 1:100; Abcam) (Pan-Montojo et al., 2010; Yasuda et al., 2011). For Western blotting, primary antibodies used were mouse anti-αSyn (clone 42; 1:150; BD Biosciences), rabbit anti-Ser^{129}-phosphorylated αSyn (ab59264; 1:500; Abcam), rabbit anti-SNAP25ct (1:1000) (Yamamori et al., 2011), mouse anti-syntaxin 1 (10H5) (1.4 μg/ml) (Yamamori et al., 2011), rabbit anti-VAMP-2 (1.4 μg/ml) (Kataoka et al., 2011), mouse anti-synaptophysin (clone SY38; 1:500; Millipore), rabbit anti-TH (1:500; Calbiochem), and rabbit anti-β-tubulin (1:500; Abcam). For immunoelectron microscopy, the primary antibodies used were mouse anti-αSyn (clone 42; 1 μg/ml; BD Biosciences), guinea pig anti-DAT (1 μg/ml; Frontier Institute), and rabbit anti-VGLUT1 (1 μg/ml; Frontier Institute).

Confocal microscopy. Free-floating sections were washed in PBS medium containing 0.05% Triton X-100 (PBS-T). As to the sections prepared from mice perfused transcardially with 2% paraformaldehyde/2% glutaraldehyde in 0.1 M PB, they were incubated with Liberate Antibody Binding (L.A.B.) solution (Polysciences) followed by washing in PBS medium and then processed in the same way as other sections. The sections were soaked with blocking agents and then incubated with the primary antibody dissolved in dilution reagent at 4°C for 48 h. Vector M.O.M. Immunodetection Kit (Vector Laboratories) was used for blocking and antibody dilution according to the instructions provided by the manufacturer. Subsequently, for fluorescent visualization of the antigens, the sections were incubated for 2 h in fresh medium containing fluorescein isothiocyanate-conjugated anti-mouse or rabbit IgG, and Cy3-conjugated anti-mouse, rabbit, goat, or rat IgG secondary antibodies (1:200–500; Jackson ImmunoResearch Laboratories). The sections were mounted on slide glass and coverslipped with Vectashield Mounting Medium with or without DAPI (Vector Laboratories). Images were captured using a confocal laser-scanning microscope (model LSM510; Zeiss) equipped with ZEN 2009 software (Zeiss) with identical settings. The software was used for image processing (brightness and contrast adjustment) applied equally to the images of wild-type and mutant mice.

Conventional electron microscopy. For conventional electron microscopy, the hemisphere brains prepared from mice perfused transcardially with 2% paraformaldehyde/2% glutaraldehyde in 0.1 M PB were post-fixed in 2% OsO_4 for 1 h. After washing in water, the samples were incubated in 2% uranyl acetate for 30 min. After dehydration using 50, 70, 90, and 100% ethanol solutions and 100% propylene oxide, the samples were embedded in Epon 812 resin (Nissin EM). Ultrathin sections were obtained using a Leica Ultracut UCT and stained with 2% uranyl acetate and lead citrate. Electron micrographs were taken with an H-7650 electron microscope (Hitachi).

Immunoelectron microscopy. For preembedding immunoelectron microscopy, parasagittal brain sections (60 μm in thickness) were incubated successively with 5% normal goat serum, primary antibodies, and peroxidase- or coloidal gold (1.4 nm)-conjugated secondary antibodies (Invitrogen). Immunoreaction was visualized with 3,3′-diaminobenzidine or silver enhancement kit (HQ silver; Nanoprobes). When combining the two methods for double immunoelectron microscopy, the brain tissue was subjected first to immunoperoxidase and then to silver-enhanced immunogold. Sections labeled by immunoperoxidase and silver-enhanced immunogold were subjected to electron microscopy as described above. The size of the nerve terminal was quantitated by using the ImageJ 1.43 software (Wayne Rasband, NIH, Bethesda, MD; http://rsb.info.nih.gov/ij).

Western blotting. Frozen striatal and ventral midbrain tissues were sonicated in chilled CelLytic-MT mammalian tissue lysis/extraction reagent (Sigma-Aldrich) mixed with protease inhibitor mixture set I (Calbiochem) and phosphatase inhibitor mixture set V (Calbiochem). The samples were centrifuged (20,000 × *g* for 10 min at 4°C), and the resulting supernatants were collected and used for Western blotting. The protein concentration in the lysate of all samples was determined using BCA protein assay kit (Pierce). Each protein sample (5–15 μg) was resolved by SDS-PAGE by means of Compact-PAGE-twin (ATTO) and then electrotransferred to Clear Blot Membrane-P (ATTO) using powered BLOT-mini (ATTO). The membrane was washed in PBS-T, incubated for 1 h in PBS-T containing 50% ChemiBLOCKER (Millipore), and then incubated for 24 h with the primary antibody in the same fresh medium. Subsequently, the membrane was incubated for 2 h in fresh medium containing horseradish peroxidase-linked anti-mouse or rabbit IgG secondary antibody (1:10,000–20,000; GE Healthcare), followed by devel-

opment of chemiluminescence using GE Healthcare ECL Plus Western Blotting Detection System (GE Healthcare). The image was captured using LAS-4000 (Fujifilm), and the signal intensity was quantitated using the ImageJ 1.43 software.

Assay for SNARE complex assembly. SNARE complex assembly was assessed by measuring the levels of the high-molecular-weight SDS-resistant complex in Western blotting performed without boiling of the samples before gel electrophoresis (Hu et al., 2002; Asuni et al., 2008; Sakisaka et al., 2008). Striatal lysate samples (15 μg of protein/sample) of wild-type and *Snap25*$^{S187A/S187A}$ mice were resolved in the SDS sample buffer. Samples were incubated for 20 min at room temperature and were further incubated at room temperature or boiled at 100°C for 3 min. Subsequently, they were analyzed by SDS-PAGE followed by the immunoblotting using the rabbit anti-SNAP25ct primary antibody (1:1000) (Yamamori et al., 2011) and horseradish peroxidase-linked anti-rabbit IgG secondary antibody (1:10,000; GE Healthcare). Except for the sample preparation before gel electrophoresis, all procedures were the same as described above (see Western blotting).

Determination of striatal levels of DA and its metabolites by HPLC. Frozen striatal tissues were sonicated in 50 mM sodium acetate. The samples were centrifuged (20,000 × *g* for 10 min at 4°C), and the resulting supernatants were mixed with equal volumes of 0.2N perchloric acid. The samples were centrifuged (20,000 × *g* for 10 min at 4°C), and the resulting supernatants were subjected to measurement of DA, homovanillic acid (HVA), and 2-(3,4-dihydroxyphenyl)-acetic acid (DOPAC) concentrations by HPLC, using an HPLC system equipped with electrochemical detection (ECD-100; EICOM; applied voltage, 500 mV) and reverse-phase column (TSK gel ODS-80TM; Tosoh). The HPLC system consisted of a pump (PU-980; Jasco; flow rate, 1.0 ml/min), autosampler (AS-1550; Jasco), column oven (860-CO; Jasco), and degasser (DG-2080–53 Jasco). The mobile phase consisted of a solution, pH 3.72, containing the following: 0.085 M $NaH_2PO_4 \cdot 2H_2O$, 2.5 mM 1-octanesulfonic acid sodium salt, 20 μM EDTA-2Na, and 15% methanol. The concentrations of DA, HVA, and DOPAC were determined in nanomoles per gram of tissue weight, and the results were expressed relative to the values of wild-type mice.

Cell count. For DA cell counting in the SN pars compacta (SNpc), every fourth 20-μm-thick serial section of the brain was immunostained for TH and counterstained with cresyl violet (Nissl staining) (Furuya et al., 2004; Yasuda et al., 2011). The numbers of TH- and Nissl-double-positive cells in the SNpc were counted both in wild-type and *Snap25*$^{S187A/S187A}$ mice in a blind manner. The SNpc cells that have nuclei optimally visible by TH immunostaining, and nuclei, cytoplasm, and nucleoli prominently stained by Nissl staining were counted. To avoid double counting of neurons with unusual shapes, TH- and Nissl-double-positive cells were counted only when their nuclei and nucleoli were optimally visualized. The rostral end of the SNpc was determined to the level where TH- and Nissl-double-positive cells began to appear (~2.60 mm caudal to the level of the bregma) (Franklin and Paxinos, 2008), and the caudal end of the SNpc was defined to the level where TH- and Nissl-double-positive cells and oculomotor nerves can be observed (~3.80 mm caudal to the level of the bregma) (Yasuda et al., 2011). In the rostral half region of the SN (~2.60–3.16 mm caudal to the level of the bregma), the SNpc was distinguished from medial ventral tegmental area (VTA) by the vertical line extended from the medial end of the cerebral peduncle. In the caudal region of the SN where the medial lemniscus can be observed (~3.16–3.80 caudal to the level of the bregma), the SNpc and medial VTA were divided along the medial lemniscus.

Statistical analysis. All data are expressed as mean ± SEM, excluding those of VGLUT1-positive nerve area, which are expressed as mean ± SD. The two-tailed Student's *t* test (for two groups) was applied. A value of $p < 0.05$ denoted the presence of statistically significant difference.

Results

Abnormal distribution of αSyn protein at presynaptic terminals in the striatum of *Snap25*$^{S187A/S187A}$ mice

Using immunohistochemistry, we investigated the distribution of endogenous αSyn in the striatum of *Snap25*$^{S187A/S187A}$ mice, which have unphosphorylatable Ala at position Ser^{187} in the SNAP-25 protein. A significant decrease of neurotransmitter release was noted in serotonergic and dopaminergic systems in the amygdala, which was associated with behavioral abnormalities, including spontaneous convulsive seizures (Kataoka et al., 2011). Confocal microscopic analysis of the striatal sections of the *Snap25*$^{S187A/S187A}$ mice showed altered distribution of endogenous αSyn, which resembled coarse granular deposits, at the age of 11 weeks, compared with age-matched wild-type control. These changes were prominent in 60-week-old (54-week-old or more was designated as aged, hereafter) *Snap25*$^{S187A/S187A}$ mice (Fig. 1*A*,*B*), indicating an age-dependent progressive manner of redistribution.

Next, we examined the localization of αSyn in the presynaptic terminals by using anti-synaptophysin antibody. Aged *Snap25*$^{S187A/S187A}$ mice showed similar alternation of the immunoreactivity for synaptophysin as observed for αSyn, compared with the wild-type (Fig. 1*C*,*D*). Moreover, αSyn-immunopositive granular structures were largely overlapped with synaptophysin. These results indicate that αSyn accumulates mainly in the presynaptic terminals in the striatum. We also analyzed the immunostaining pattern for Ser^{129}-phosphorylated αSyn (p-αSyn), which was found specifically in human α-synucleinopathies (Fujiwara et al., 2002). Majority of αSyn-positive granular deposits were immunopositive for p-αSyn, which were detected at negligible amounts in wild-type control mice (Fig. 1*F*,*G*). These results indicate that the abnormal accumulation of αSyn in the striatum of *Snap25*$^{S187A/S187A}$ mice represents in part the pathological changes in human DLB brains.

Abnormal accumulation of αSyn and p-αSyn proteins in the striatum of *Snap25*$^{S187A/S187A}$ mice

Next, we measured αSyn and p-αSyn protein levels in the striatal tissues of aged *Snap25*$^{S187A/S187A}$ mice. A significant decrease of SNAP-25 protein was found in *Snap25*$^{S187A/S187A}$ mice ($p < 0.0001$) compared with age-matched wild-type mice, confirming our previous findings (Kataoka et al., 2011). Importantly, αSyn (~1.5-fold; $p = 0.0047$) and p-αSyn (~1.7-fold; $p = 0.0080$) protein levels were higher than age-matched wild-type mice (Fig. 2*A*,*B*). These results indicate that the abnormal distribution of αSyn and p-αSyn in the presynaptic terminals (Fig. 1*F*) was reflected by increased amount of these proteins. In addition, high levels of VAMP-2 (~1.3-fold; $p = 0.0011$), but neither syntaxin nor synaptophysin, were found in the striatum of aged *Snap25*$^{S187A/S187A}$ mice (Fig. 2*A*,*B*), compared with whole-brain lysate prepared from young *Snap25*$^{S187A/S187A}$ mice (Kataoka et al., 2011).

Ultrastructural analysis of αSyn distribution in presynaptic terminals

To investigate in detail the morphological changes in the presynaptic terminals, we used electron microscopy to analyze the striatum of the aged mice. In *Snap25*$^{S187A/S187A}$ mice, condensed synaptic vesicles were abundantly present in large excitatory nerve terminals, compared with the normal uniform distribution of the vesicles in wild-type mice (Fig. 3*A*,*B*). These results suggest possible decrease of presynaptic neurotransmitter release in *Snap25*$^{S187A/S187A}$ mice. Subsequent immunoelectron-microscopic examination of αSyn in the synapses showed predominant localization of αSyn proteins in the periactive zone of enlarged excitatory presynaptic nerve terminals in the aged *Snap25*$^{S187A/S187A}$ mice, compared with the wild type (Fig. 3*C*,*D*).

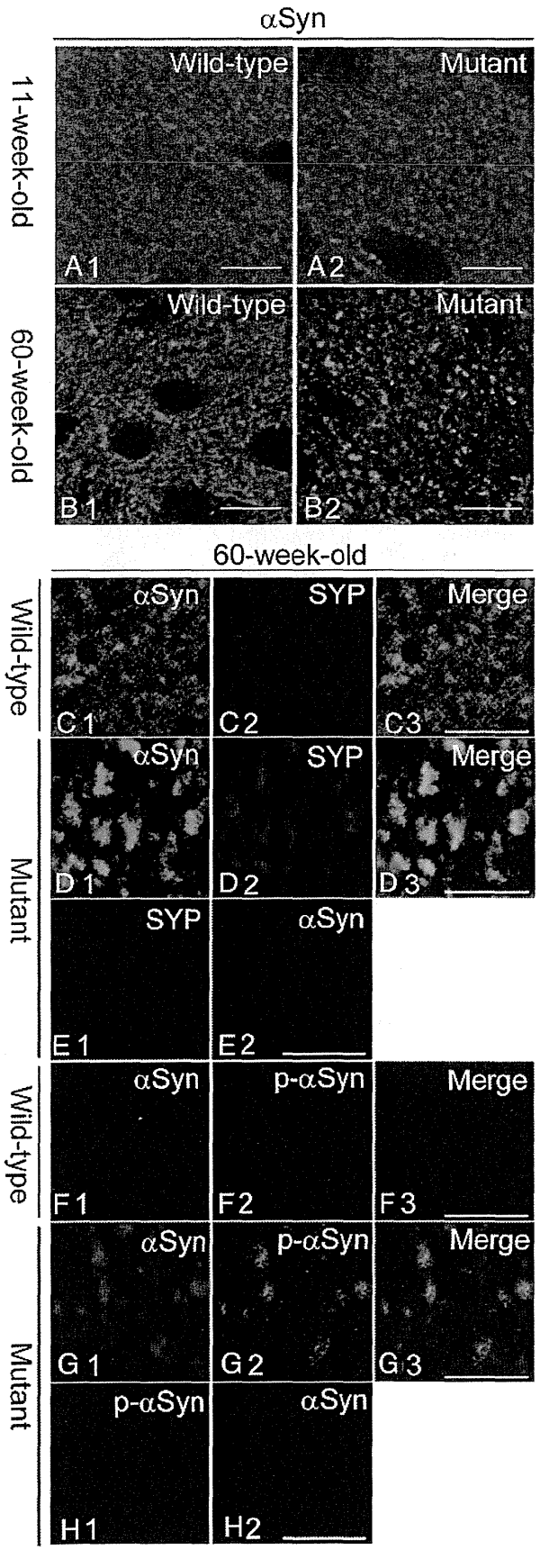

Figure 1. Altered localization of αSyn and its accumulation in presynaptic terminals in the striatum of *Snap25*$^{S187A/S187A}$ mice. ***A***, ***B***, Striatal sections of wild-type and *Snap25*$^{S187A/S187A}$ (mutant) mice at postnatal weeks 11 and 60 were immunostained for αSyn ($n = 3$ for each genotype). Compared with the wild-type mice (***A***$_1$, ***B***$_1$), αSyn was localized and formed coarse granular deposits in mutant mice at postnatal weeks 11 and 60 (***A***$_2$, ***B***$_2$). The severity of the change was more prominent at postnatal week 60. Scale bars, 10 μm. ***C–H***, Sections were coimmunostained for αSyn, and synaptophysin (SYP) or p-αSyn. Confocal images showed altered localization of SYP (***D***$_2$) and p-αSyn (***G***$_2$) and colocalization with αSyn-positive coarse granular deposits (***D***$_1$, ***G***$_1$) in mutant mice (***D***$_3$, ***G***$_3$). No cross-reactivity was observed for the sections of the mutant mice exposed to a single primary antibody followed by the treatment of both secondary antibodies were observed (***E***$_1$, ***E***$_2$, ***H***$_1$, ***H***$_2$) [i.e., negligible green (***E***$_1$) and red fluorescence (***E***$_2$) for the sections treated with anti-SYP and αSyn antibody, respectively]. Scale bars, 5 μm.

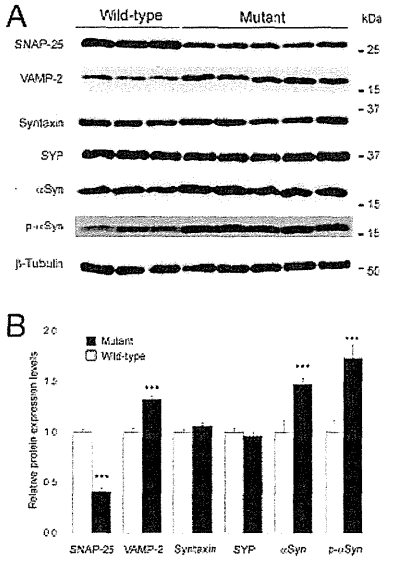

Figure 2. Increase in endogenous αSyn and p-αSyn in the striatum of *Snap25*$^{S187A/S187A}$ mice. ***A***, ***B***, Western blotting was performed for synaptic marker proteins using the striatal tissues at postnatal week 61. ***A***, Representative Western blotting images of two to five independent experiments, each involving three and five mice for wild-type and *Snap25*$^{S187A/S187A}$ (mutant), respectively. Mutant mice showed increased band intensity of αSyn, p-αSyn, and VAMP-2 compared with the wild type, while that of SNAP-25 was decreased. ***B***, Relative protein expression levels expressed relative to the loading control (β-tubulin). The band intensity was quantitated using the ImageJ 1.43 software and expressed as the relative protein expression level. Significant increases in α-Syn, p-αSyn, and VAMP-2, and significant decrease in SNAP-25 were observed in mutant mice. No significant differences were noted in other synaptic protein markers. Data are mean ± SEM of two to five independent experiments, each involving three and five mice for wild-type and mutant, respectively. ***$p < 0.01$ (two-tailed t test).

Decreased ability of SNARE complex assembly in *Snap25*$^{S187A/S187A}$ mice

Given that *Snap25*$^{S187A/S187A}$ mice clearly displayed the significant decrease in the SNAP-25 protein expression and abnormal distribution of the synaptic vesicle in the presynaptic terminals (Figs. 2, 3*B*), we evaluated the functional ability to produce the SNARE complex in *Snap25*$^{S187A/S187A}$ mice. SNARE complex assembly was assessed by measuring the levels of the high-molecular-weight heat-sensitive SDS-resistant complex in Western blotting. As shown in Figure 4*A*, compared with boiled sample of the wild type, SNAP-25-immunoreactive bands were shifted to the higher molecular masses (~75 to ~250 kDa) in unboiled samples of wild-type and *Snap25*$^{S187A/S187A}$ mice. However, the relative signal intensity of higher molecular masses normalized by β-tubulin (loading control) was significantly reduced in *Snap25*$^{S187A/S187A}$ mice, compared with the wild-type mice ($p = 0.00463$) (Fig. 4*B*). These observations indi-

cated the decreased ability of the SNARE complex assembly in *Snap25*$^{S187A/S187A}$ mice compared with the wild-type mice. This is considered to represent the functional deficit possibly attributable to the decreased level of the SNAP-25 and the insensitivity of protein kinase C-mediated phosphorylation at Ser^{187} in *Snap25*$^{S187A/S187A}$ mice.

αSyn accumulation and enlargement of corticostriatal nerve terminals

The striatal spiny interneurons receive excitatory outputs from cortical and thalamic tracts, and these projections use glutamate as the neurotransmitter (Gerfen and Surmeier, 2011). VGLUT1 and VGLUT2 are localized to the excitatory nerve terminals projecting from the cortical and the thalamic area, respectively, in the striatum. Then, we investigated the distribution of αSyn-immunopositive deposits with VGLUT1 or VGLUT2 to verify the abnormal accumulation of αSyn in the corticostriatal or the thalamostriatal neuronal terminals. As shown in Figure 5B_2, we found similar alternation of the immunoreactivity for VGLUT1 as observed for αSyn in the aged *Snap25*$^{S187A/S187A}$ mice compared with wild-type normal ones (Fig. 5A_2). Importantly, such immunoreactivity for VGLUT1, but not for VGLUT2, was exclusively colocalized with αSyn (Fig. 5B_3,E_3). We also performed double immunostaining with anti-pSyn and anti-VGLUT1 antibodies and found the VGLUT1-immunopositive structures to be immunopositive for p-αSyn (Fig. 5G_3). These observations suggest accumulation of αSyn and p-αSyn mainly in the enlarged VGLUT1-positive nerve terminals.

Immunoelectron-microscopic examination showed massive enlargement of the VGLUT1-positive nerve terminals in the aged *Snap25*$^{S187A/S187A}$ mice (Fig. 5*I*,*J*). Quantitative analysis of the size of the VGLUT1-positive nerve terminals based on the cumulative probability curve confirmed a significantly larger size in *Snap25*$^{S187A/S187A}$ mice compared with wild-type mice (Fig. 5*K*). The size of the VGLUT1-positive nerve terminals reached a plateau at 0.8 μm^2 in wild-type mice, while that of *Snap25*$^{S187A/S187A}$ mice reached a plateau at 3.6 μm^2. The size of ~40% of the VGLUT1-positive nerve terminals in the mutant mice was larger than the maximum size measured in wild-type mice. Specifically, the size of the VGLUT1-positive nerve terminals in the mutant mice was approximately fourfold larger than the wild type ($p = 0.0030$) (Fig. 5*L*).

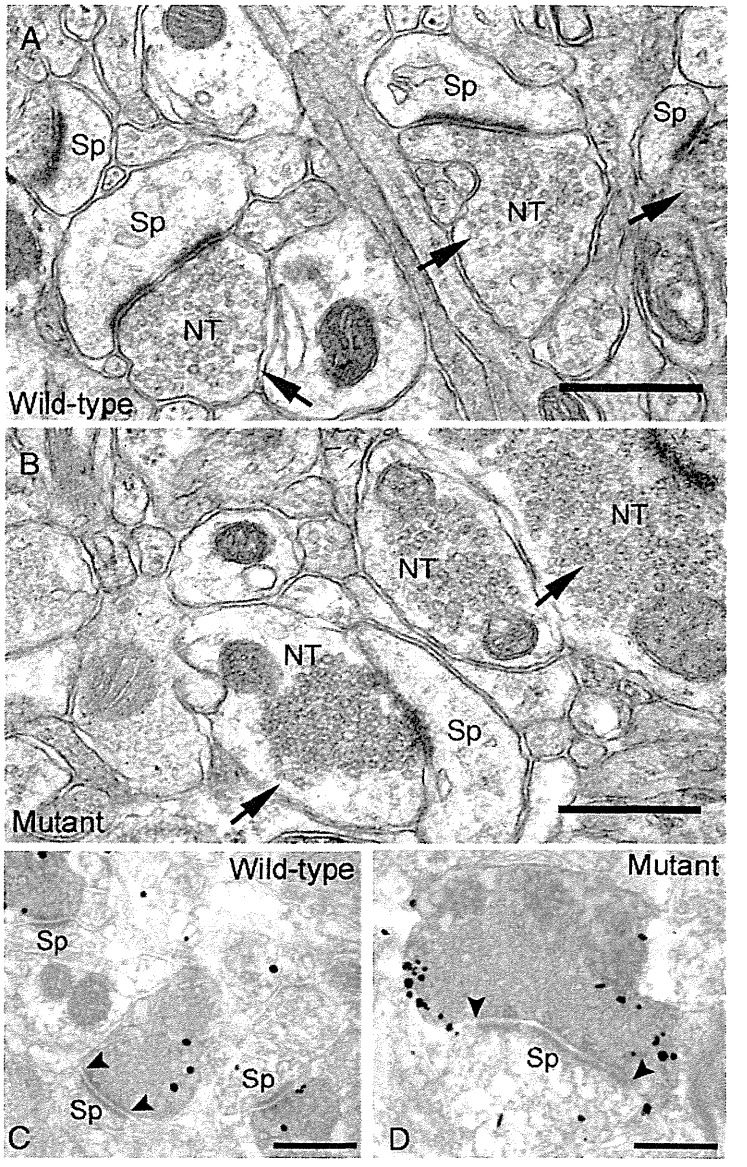

Figure 3. Abnormal excitatory nerve terminals in the striatum of *Snap25*$^{S187A/S187A}$ (mutant) mice. Representative electron micrographs of wild-type and mutant mice at postnatal week 60 ($n = 3$ for each genotype). Synaptic vesicles were homogeneously distributed in the cytoplasm of the excitatory nerve terminals in wild-type mice (***A***), while they were tightly assembled in mutant mice (***B***). Note the alteration of subcellular localization of α-Syn (immunogold particles) and increased number of αSyn aggregates deposited in association with the cytoplasmic face of the plasma membrane at the periactive zone of the enlarged nerve terminals in mutant mice (***D***), but not in wild-type mice (***C***). Arrows, excitatory nerve terminals; arrowheads, edges of active zone. NT, Nerve terminal; Sp, dendritic spine. Scale bars, 500 nm.

No significant changes in nigrostriatal dopaminergic system

Finally, we examined the effect of SNARE dysfunction on the nigrostriatal dopaminergic system, which is affected in parkinsonian brains. The striatal sections of aged *Snap25*$^{S187A/S187A}$ mice were co-immunostained for αSyn and dopaminergic neuronal markers (TH or DAT). The αSyn-immunopositive deposits appeared adjacent to, but hardly colocalized with both DAT and TH in *Snap25*$^{S187A/S187A}$ mice. The distribution patterns of DAT- and TH-immunoreactive deposits in the striatum were not significantly different between wild-type and mutant mice (Fig. 6*A–D*). These results imply that the nigrostriatal dopaminergic neurons are not affected in *Snap25*$^{S187A/S187A}$ mice.

To clarify this point further, we conducted immunoelectron-microscopic examination of DAT-positive dopaminergic nerve terminals. There were no significant differences in any structural alternations including condensation of synaptic vesicles (Fig. 6*E*,*F*). Furthermore, we found no significant differences in the subcellular localization of αSyn protein between the aged wild-type and *Snap25*$^{S187A/S187A}$ mice (Fig. 6*G*,*H*).

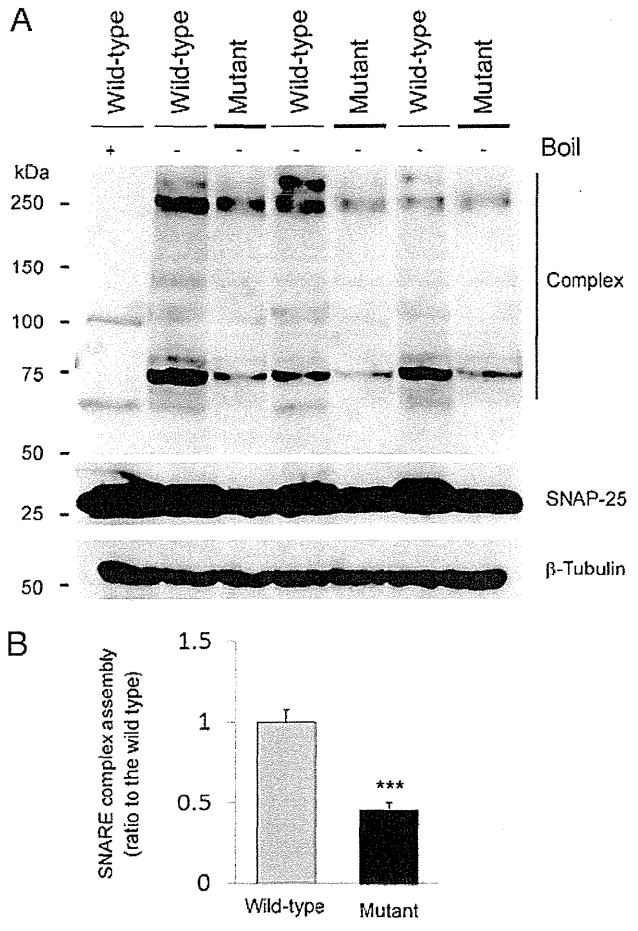

Figure 4. Decreased ability of the SNARE complex assembly in *Snap25*$^{S187A/S187A}$ (mutant) mice. ***A***, ***B***, Western blotting was performed for unboiled or boiled samples of wild-type and mutant mice (at postnatal week 61) before electrophoresis followed by the immunoblotting using SNAP-25ct antibody. ***A***, Representative Western blotting image of two to three independent experiments was provided. Heat-sensitive SDS-resistant SNAP-25ct-immunoreactive bands were detected at high molecular mass (~75 to ~250 kDa) in wild-type and mutant mice, indicating the presence of the SNARE complex. However, band intensity of the mutant mice, especially at ~75 kDa, was decreased compared with the wild-type mice. ***B***, Relative levels of the SNARE complex assembly relative to the loading control (β-tubulin). The band intensity was quantitated using the ImageJ 1.43 software and expressed as the relative protein expression level. Significant decrease in SNARE complex assembly was observed in mutant mice compared with the wild-type mice. Data are mean ± SEM of two to three independent experiments, each involving three mice for each genotype. ***$p < 0.01$ (two-tailed t test).

We also investigated the functional preservation of the nigrostriatal dopaminergic neurons in the aged *Snap25*$^{S187A/S187A}$ mice. No significant difference was found in the number of TH- and Nissl-double-positive cells in the SNpc between wild-type and *Snap25*$^{S187A/S187A}$ mice (Fig. 6*I*,*J*). There were also no significant differences in the levels of TH protein in the midbrain tissue and DA and its metabolites, HVA and DOPAC, in the striatum between the aged wild-type and *Snap25*$^{S187A/S187A}$ mice (Fig. 6*K*–*M*). These results suggest that SNARE dysfunction does not seem to be involved in the initiation of PD-related pathologic changes in nigrostriatal dopaminergic neurons.

Discussion

In this study, we found that SNARE dysfunction leads to presynaptic accumulation of endogenous αSyn, a process that probably represents the initial pathological event in DLB. Previous studies using neural preparations showed that the neurotransmitter release is regulated by protein kinase C, which phosphorylates Ser^{187} residue in SNAP-25, augmenting exocytosis of synaptic vesicles (Majewski and Iannazzo, 1998; Morgan et al., 2005). Patch-clamp analysis of chromaffin cells that overexpress the S187A form of SNAP-25 inhibited the rate of refilling of presynaptic vesicle pool (Nagy et al., 2002). Recently, we reported that *Snap25*$^{S187A/S187A}$ mice show reduced DA and serotonin release in amygdala (Kataoka et al., 2011). In human DLB brains, >90% of αSyn aggregates are located in the presynaptic terminals in the form of small deposits (Neumann et al., 2002; Kramer and Schulz-Schaeffer, 2007; Schulz-Schaeffer, 2010). This is consistent with the present findings of abnormal accumulation of αSyn in presynapses, suggesting that this process is the initial pathological event in DLB, eventually leading to the death and degeneration of neuronal cells (Orimo et al., 2008). Another finding that lends support to the role of αSyn aggregates in the presynaptic terminals in DLB was the lack of histopathological changes in the dopaminergic terminals in the present study.

In experiments on glutamate release conducted in hippocampal slices prepared from αSyn knock-out mice (Gureviciene et al., 2007), paired-pulse facilitation was significantly weaker, and high-frequency-induced long-term potentiation and frequency facilitation were not observed. These findings suggest that αSyn contributes to mobilization of glutamate-containing vesicles from the reserve pool (Gureviciene et al., 2007). Thus, αSyn may act as a positive regulator of neurotransmitter release at presynaptic terminals. Therefore, presynaptic accumulation of αSyn observed in *Snap25*$^{S187A/S187A}$ mice might reflect a compensatory response to a possible SNARE dysfunction-related chronic shortage of neurotransmitter release in the VGLUT1-positive nerve terminals.

In the striatum, the medium spiny neurons, which constitute >90% of all striatal neurons, receive output from glutamatergic axons that contact the spine head and dopaminergic axons that synapse with the dendritic spine neck. DA released from dopaminergic axons regulates the release of glutamate via D_2-like receptors on the corticostriatal nerve terminals (Bamford et al., 2004; Wickens and Arbuthnott, 2005). In the present study, we found no significant changes in the striatal tissue levels of DA and its metabolites. These findings confirmed the results reported in our previous study using *Snap25*$^{S187A/S187A}$ mice, whereas microdialysis analysis study revealed marked reduction of DA release from the amygdala (not measured in other brain regions) (Kataoka et al., 2011). In addition, in another *in vitro* study using PC12 cells, phosphorylation of SNAP-25 at S187 potentiated calcium-dependent DA release and recruitment of synaptic vesicles containing DA (Shimazaki et al., 1996; Iwasaki et al., 2000; Shoji-Kasai et al., 2002). These observations suggest decreased striatal DA release in *Snap25*$^{S187A/S187A}$ mice, resulting in increased demand for neurotransmitter release at glutamatergic nerve terminals. Thus, presynaptic accumulation of αSyn might reflect a possible compensatory response to low DA inhibitory control over cortical glutamatergic drive.

Increased expression of VAMP-2 protein accompanied increased αSyn expression in the striatum of *Snap25*$^{S187A/S187A}$ mice. Binding of the C terminus of αSyn to the N terminus of VAMP-2 primes the subsequent SNARE complex assembly (Burgoyne and Morgan, 2011). Therefore, the increased VAMP-2 level might also reflect a compensatory response to the impaired synaptic vesicle release by enhancing SNARE complex formation in concert with the increased αSyn.

Presynaptic neurotransmitter release is mediated by the synaptic vesicle cycle, consisting of exocytosis followed by en-

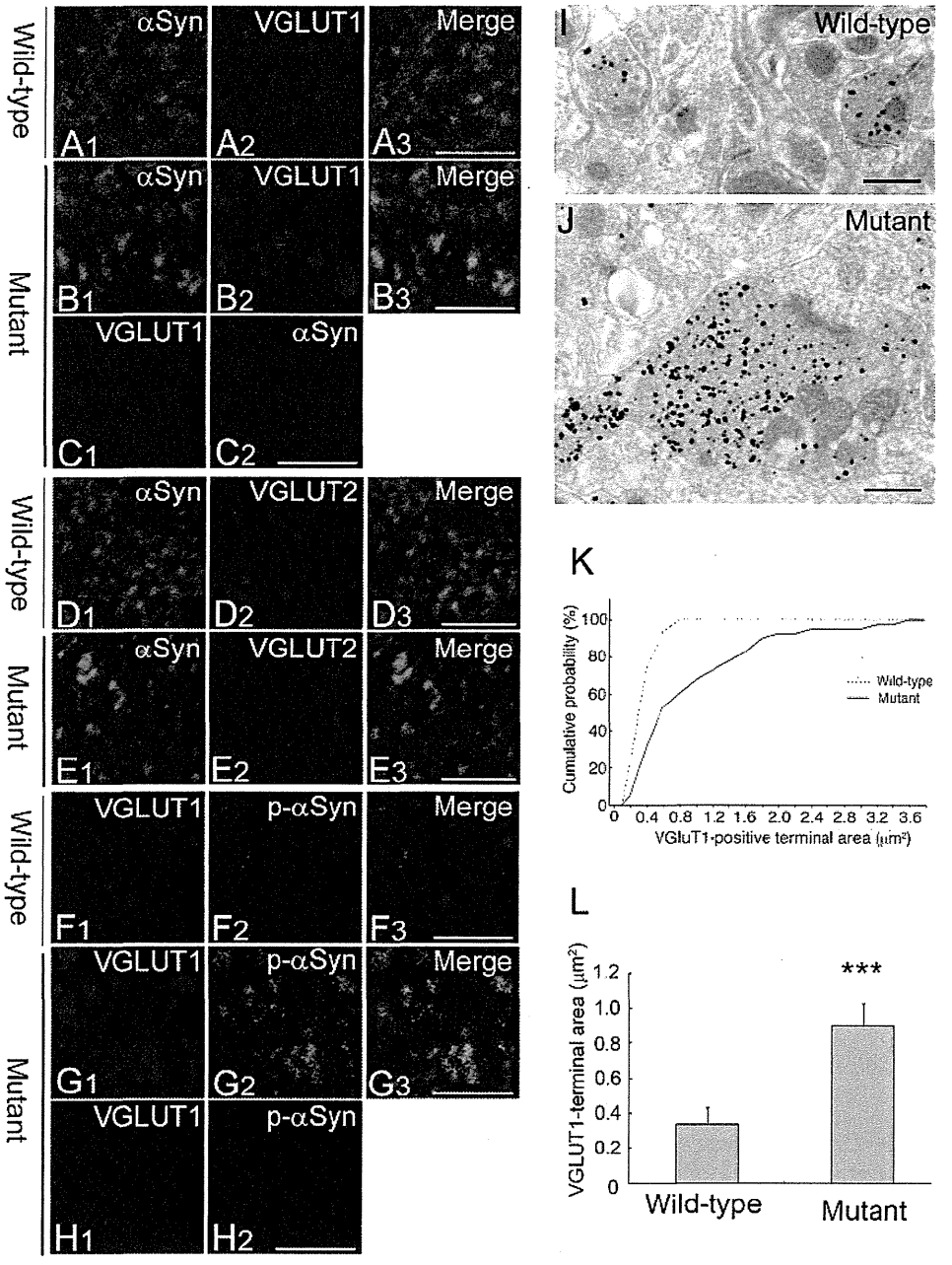

Figure 5. Accumulation of αSyn in the hypertrophied VGLUT1-positive nerve terminals. ***A–E***, Striatal sections of wild-type and *Snap25*$^{S187A/S187A}$ (mutant) mice at postnatal week 60 were coimmunostained for αSyn (green) and VGLUT1 or VGLUT2 (red) ($n = 3$ for each genotype). Confocal images showed altered localization of VGLUT1 with more granular appearance in mutant mice (***B***$_2$) compared with wild-type mice (***A***$_2$). Immunopositive structures for VGLUT1, but not for VGLUT2, marked colocalization with αSyn-positive granular deposits (***B***$_3$, ***E***$_3$). No cross-reactivity was observed for the sections of the mutant mice treated with a single antibody followed by both the secondary antibodies, as evidenced by negligible green (***C***$_1$) and red fluorescence (***C***$_2$) for the sections treated with anti-VGLUT1 and αSyn antibody, respectively. Scale bars, 5 μm. ***F–H***, Sections were coimmunostained for VGLUT1 (red) and p-αSyn (green) ($n = 3$ for each genotype). Confocal images showed marked colocalization of VGLUT1 and p-αSyn in mutant mice (***G***$_3$). Similarly, no cross-reactivity was observed as evidenced by negligible red (***H***$_1$) and green fluorescence (***H***$_2$) for the sections treated with anti-VGLUT1 and αSyn antibody, respectively. Scale bars, 5 μm. ***I***, ***J***, Representative electron micrographs showing VGLUT1-positive nerve terminals (labeled with immunogold particles). Note the hypertrophy of VGLUT1-positive nerve terminals in mutant mice (***J***), but not in wild-type mice (***I***). Scale bars, 500 nm. ***K***, ***L***, Quantitative analysis of VGLUT1-positive nerve terminal area in three mice per group. The size was measured in 100 nerve terminals per animal. Cumulative probability (***K***) and group mean value (***L***) were calculated and showed a larger nerve terminal area in mutant mice than the wild type. Data are mean ± SD. ***$p < 0.01$ (two-tailed t test).

docytosis and recycling. Exocytosis incorporates synaptic vesicles into the presynaptic terminal membranes and increases the surface area, while endocytosis retrieves the excess plasma membrane components followed by recycling to form other synaptic vesicles. Under normal conditions, the dynamics of the balance between exocytosis and endocytosis is well preserved to maintain the correct surface area of the presynaptic terminal (Hayes and Baines, 1996; Haucke et al., 2011). However, excessive accumulation of presynaptic vesicles and enlargement of the VGLT1-positive nerve terminals was observed in *Snap25*$^{S187A/S187A}$ mice. Taking into consideration the synaptic vesicle cycle, our findings suggest that the balance of the cycle was biased toward decreased exocytosis concomitant with possible decreased endocytosis.

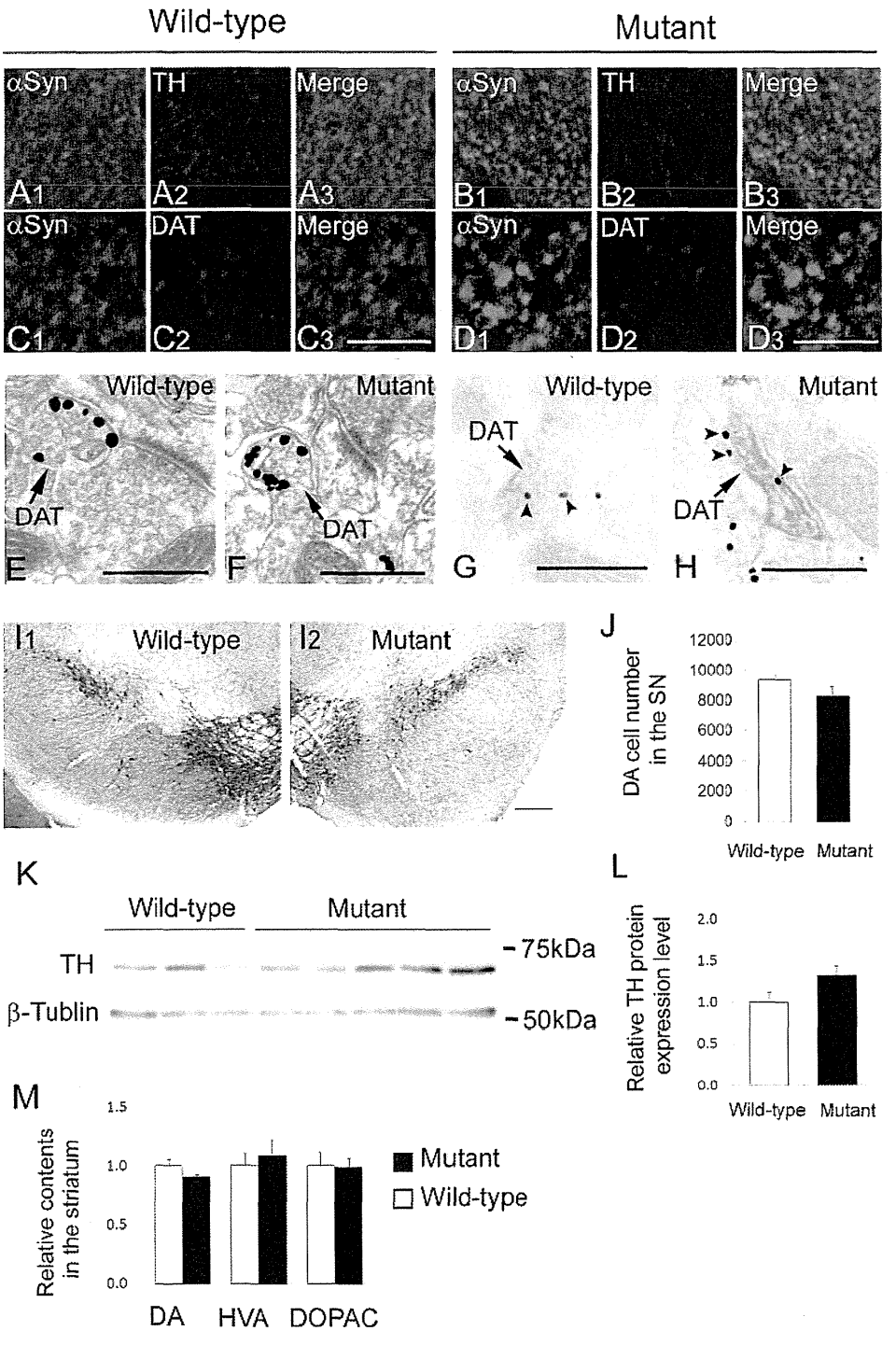

Figure 6. Lack of neurodegenerative changes in nigrostriatal dopaminergic neurons. ***A–D***, Striatal sections of wild-type and *Snap25*$^{S187A/S187A}$ (mutant) mice at postnatal week 60 were coimmunostained for α-Syn (green) and TH or DAT (red) ($n = 3$ for each genotype). There were no significant differences in the distribution pattern of TH (***A***$_2$, ***B***$_2$) and DAT (***C***$_2$, ***D***$_2$) between wild-type and mutant mice. αSyn-positive granular deposits (***B***$_1$, ***D***$_1$) were rarely colocalized with TH or DAT (***B***$_3$, ***D***$_3$). Scale bars, 5 μm. ***E–H***, Representative electron micrographs of dopaminergic nerve terminals at postnatal week 60 ($n = 3$ for each genotype). They were identified by silver particles (***E***, ***F***) or DAB labeling (***G***, ***H***) for DAT (arrows). There were no significant differences in subcellular localization of synaptic vesicles (***E***, ***F***) or αSyn (arrowheads, silver particles) (***G***, ***H***) between wild-type and mutant mice. Scale bars, 500 nm. ***I***, ***J***, Representative micrographs of the substantia nigra of wild-type and mutant mice at postnatal week 60 immunostained for TH and counterstained with cresyl violet. Scale bars: ***I***$_1$, ***I***$_2$, 200 μm. Number of DA cell bodies counted in three mice of each genotype. Data are mean ± SEM (***J***). ***K***, ***L***, Western blotting was performed using substantia nigral tissues at postnatal week 61. Representative images of Western blotting from two independent experiments, each involving three and five mice of wild-type and mutant mice, respectively (***K***). Relative TH protein expression levels (relative to the expression of β-tubulin) were expressed relative to the value of wild-type mice (***L***). Data are mean ± SEM of two independent experiments, each involving three and five mice of wild-type and mutant, respectively. ***M***, Quantification of DA, HVA, and DOPAC levels in the striatum of mice at postnatal week 54. Data were expressed relative to those of wild-type mice and represent the mean ± SEM of duplicate measurement of one experiment involving four mice of each genotype. There were no significant differences between wild-type and mutant mice (***J***, ***L***, ***M***) (two-tailed *t* test).

The enlarged VGLUT1-positive nerve terminals of *Snap25*$^{S187A/S187A}$ mice showed concomitant accumulation of αSyn and p-αSyn. Kramer and Schulz-Schaeffer (2007) have previously reported that 90% or even more of αSyn aggregates in DLB cases were located at the presynapses in the form of very small deposits. In parallel, dendritic spines were retracted, whereas the presynapses were relatively preserved, suggesting that a neurotransmitter deprivation may explain the cognitive impairment in DLB (Kramer and Schulz-Schaeffer, 2007; Schulz-Schaeffer, 2010). While the presynaptic aggregates did not contain much p-αSyn in their examination (Kramer and Schulz-Schaeffer, 2007; Schulz-Schaeffer, 2010), widespread varicosities and dot-like structures containing p-αSyn are commonly observed in mouse model and human DLB brains (Saito et al., 2003; Scott et al., 2010). This may represent axonal transport defects and presynaptic dysfunctions (Saito et al., 2003; Scott et al., 2010). Recent study showed that mutant αSyn (A53T) diminished levels of various motor proteins in neurons (Chung et al., 2009), supporting this scenario. Alternatively, excessive amounts of misfolded αSyn and p-αSyn may aggregate at synapses, physically preventing the targeting of other presynaptic proteins (Kramer and Schulz-Schaeffer, 2007). In experiments using *Caenorhabditis elegans* overexpressing the human αSyn, four genes related to the endocytosis process were identified as genetic modifiers for αSyn toxicity (Kuwahara et al., 2008). They included the two subunits of the adaptor protein (AP) complex 2, which interacts with clathrin and promotes presynaptic clathrin-mediated vesicle recycling (Morgan et al., 2000). Furthermore, proteomics analysis revealed that p-αSyn also preferentially interacted with the proteins involved in endocytosis, including clathrin heavy chain and subunit of AP-2 and AP-1 complexes, over the nonphosphorylated αSyn (McFarland et al., 2008). Clathrin-mediated recycling of exocytosed synaptic vesicles occurs in the periactive zone, a region adjacent to the active zone where synaptic vesicle is endocytosed (Haucke et al., 2011). Similarly, in *Snap25*$^{S187A/S187A}$ mice, immunoelectron microscopy showed preferential localization of αSyn at the periactive zone of the excitatory presynaptic nerve terminals (Fig. 3*D*). This might reflect the interaction of αSyn and p-αSyn with the proteins involved in clathrin-mediated endocytosis. Taking these findings together, presynaptic accumulation of αSyn and p-αSyn could disturb the endocytosis process and consequently contribute to the development of VGLUT1-positive terminal enlargement.

Presynaptic accumulation of αSyn is considered an early event in the pathogenesis of α-synucleinopathies (Neumann et al., 2002; Kramer and Schulz-Schaeffer, 2007; Schulz-Schaeffer, 2010). Mice overexpressing human αSyn showed presynaptic accumulation of αSyn and low DA release in the striatum. These findings were associated with abnormal distribution of SNARE proteins, which colocalized with αSyn aggregates. Similarly, accumulation of SNARE proteins and αSyn were reported in the striatum of PD patients (Garcia-Reitböck et al., 2010). These observations suggest that SNARE dysfunction likely occurs at an early stage of pathogenesis in nigrostriatal dysfunction observed in PD. By considering the findings observed in the VGLUT1-positive nerve terminals, we expected that SNARE dysfunction might have induced presynaptic accumulation of αSyn, which consequently results in the development of neurodegenerative changes in the nigrostriatal system. However, contrary to our expectation, *Snap25*$^{S187A/S187A}$ mice showed no significant neurodegenerative changes in nigrostriatal dopaminergic neurons, suggesting that SNARE dysfunction alone was insufficient to cause nigrostriatal degeneration as observed in PD, and appeared to be a downstream event associated with abnormal accumulation of αSyn.

In conclusion, the present study demonstrated that SNARE dysfunction leads to accumulation of endogenous αSyn in the corticostriatal nerve terminals. Presynaptic accumulation of αSyn is considered to be a key early event in the pathogenesis of α-synucleinopathies. Although the "prion-like" propagation hypothesis of αSyn, including tau and TAR DNA-binding protein 43 kDa, is currently receiving considerable attention worldwide, our findings provide an insight to our understanding of the possible mechanisms that lead to presynaptic accumulation of endogenous αSyn. Moreover, given that SNAP-25 is reduced in the striatum of MSA brains (Tong et al., 2010), we speculate that a discontinuous pattern of αSyn pathologies usually found in MSA [i.e., glial cytoplasmic inclusions in the putaminal oligodendrocytes, and neuronal cytoplasmic inclusions and neuronal nuclear inclusions in the cortex (Yoshida, 2007; Ubhi et al., 2011)] might be potentially linked through the presynaptic accumulation of αSyn in the corticostriatal neurons. Further investigations on the *Snap25* mutant mice with genetic ablation of αSyn would contribute to understanding the essential role of redistributed αSyn and should be a central issue in the following studies.

References

Asuni AA, Cunningham C, Vigneswaran P, Perry VH, O'Connor V (2008) Unaltered SNARE complex formation in an in vivo model of prion disease. Brain Res 1233:1–7. CrossRef Medline

Bamford NS, Robinson S, Palmiter RD, Joyce JA, Moore C, Meshul CK (2004) Dopamine modulates release from corticostriatal terminals. J Neurosci 24:9541–9552. CrossRef Medline

Burgoyne RD, Morgan A (2011) Chaperoning the SNAREs: a role in preventing neurodegeneration? Nat Cell Biol 13:8–9. CrossRef Medline

Burré J, Sharma M, Tsetsenis T, Buchman V, Etherton MR, Südhof TC (2010) Alpha-synuclein promotes SNARE-complex assembly in vivo and in vitro. Science 329:1663–1667. CrossRef Medline

Cabin DE, Shimazu K, Murphy D, Cole NB, Gottschalk W, McIlwain KL, Orrison B, Chen A, Ellis CE, Paylor R, Lu B, Nussbaum RL (2002) Synaptic vesicle depletion correlates with attenuated synaptic responses to prolonged repetitive stimulation in mice lacking α-synuclein. J Neurosci 22:8797–8807. Medline

Chandra S, Gallardo G, Fernández-Chacón R, Schlüter OM, Südhof TC (2005) Alpha-synuclein cooperates with CSPalpha in preventing neurodegeneration. Cell 123:383–396. CrossRef Medline

Chung CY, Koprich JB, Siddiqi H, Isacson O (2009) Dynamic changes in presynaptic and axonal transport proteins combined with striatal neuroinflammation precede dopaminergic neuronal loss in a rat model of AAV α-synucleinopathy. J Neurosci 29:3365–3373. CrossRef Medline

Chung YH, Joo KM, Kim MJ, Cha CI (2003) Immunohistochemical study on the distribution of alpha-synuclein in the central nervous system of transgenic mice expressing a human Cu/Zn superoxide dismutase mutation. Neurosci Lett 342:151–154. CrossRef Medline

Darios F, Ruipérez V, López I, Villanueva J, Gutierrez LM, Davletov B (2010) Alpha-synuclein sequesters arachidonic acid to modulate SNARE-mediated exocytosis. EMBO Rep 11:528–533. CrossRef Medline

Franklin KBJ, Paxinos G (2008) The mouse brain in stereotaxic coordinates, Ed 3. New York: Academic.

Fujiwara H, Hasegawa M, Dohmae N, Kawashima A, Masliah E, Goldberg MS, Shen J, Takio K, Iwatsubo T (2002) alpha-Synuclein is phosphorylated in synucleinopathy lesions. Nat Cell Biol 4:160–164. Medline

Furuya T, Hayakawa H, Yamada M, Yoshimi K, Hisahara S, Miura M, Mizuno Y, Mochizuki H (2004) Caspase-11 mediates inflammatory dopaminergic cell death in the 1-methyl-4-phenyl-1,2,3,6-tetrahydropyridine mouse model of Parkinson's disease. J Neurosci 24:1865–1872. CrossRef Medline

Galvin JE, Lee VM, Trojanowski JQ (2001) Synucleinopathies: clinical and pathological implications. Arch Neurol 58:186–190. CrossRef Medline

Garcia-Reitböck P, Anichtchik O, Bellucci A, Iovino M, Ballini C, Fineberg E, Ghetti B, Della Corte L, Spano P, Tofaris GK, Goedert M, Spillantini MG (2010) SNARE protein redistribution and synaptic failure in a transgenic mouse model of Parkinson's disease. Brain 133:2032–2044. CrossRef Medline

Gerfen CR, Surmeier DJ (2011) Modulation of striatal projection systems by dopamine. Annu Rev Neurosci 34:441–466. CrossRef Medline

Gimbel DA, Nygaard HB, Coffey EE, Gunther EC, Laurén J, Gimbel ZA, Strittmatter SM (2010) Memory Impairment in transgenic Alzheimer mice requires cellular prion protein. J Neurosci 30:6367–6374. CrossRef Medline

Gureviciene I, Gurevicius K, Tanila H (2007) Role of alpha-synuclein in synaptic glutamate release. Neurobiol Dis 28:83–89. CrossRef Medline

Haucke V, Neher E, Sigrist SJ (2011) Protein scaffolds in the coupling of synaptic exocytosis and endocytosis. Nat Rev Neurosci 12:127–138. CrossRef Medline

Hayes NVL, Baines AJ (1996) Small synaptic vesicles. In: Biomembranes: a multi-volume treatise (Lee AG, ed), pp 75–122. Greenwich, CT: JAI.

Herzig MC, Kolly C, Persohn E, Theil D, Schweizer T, Hafner T, Stemmelen C, Troxler TJ, Schmid P, Danner S, Schnell CR, Mueller M, Kinzel B, Grevot A, Bolognani F, Stirn M, Kuhn RR, Kaupmann K, van der Putten PH, Rovelli G, et al. (2011) LRRK2 protein levels are determined by kinase function and are crucial for kidney and lung homeostasis in mice. Hum Mol Genet 20:4209–4223. CrossRef Medline

Hu K, Carroll J, Rickman C, Davletov B (2002) Action of Complexin on SNARE complex. J Biol Chem 277:41652–41656. CrossRef Medline

Iwai A, Masliah E, Yoshimoto M, Ge N, Flanagan L, de Silva HA, Kittel A, Saitoh T (1995) The precursor protein of non-A beta component of Alzheimer's disease amyloid is a presynaptic protein of the central nervous system. Neuron 14:467–475. CrossRef Medline

Iwasaki S, Kataoka M, Sekiguchi M, Shimazaki Y, Sato K, Takahashi M (2000) Two distinct mechanisms underlie the stimulation of neurotransmitter release by phorbol esters in clonal rat pheochromocytoma PC12 cells. J Biochem 128:407–414. CrossRef Medline

Kataoka M, Yamamori S, Suzuki E, Watanabe S, Sato T, Miyaoka H, Azuma S, Ikegami S, Kuwahara R, Suzuki-Migishima R, Nakahara Y, Nihonmatsu I, Inokuchi K, Katoh-Fukui Y, Yokoyama M, Takahashi M (2011) A single amino acid mutation in SNAP-25 induces anxiety-related behavior in mouse. PLoS One 6:e25158. CrossRef Medline

Kaushal N, Seminerio MJ, Shaikh J, Medina MA, Mesangeau C, Wilson LL, McCurdy CR, Matsumoto RR (2011) CM156, a high affinity sigma ligand, attenuates the stimulant and neurotoxic effects of methamphetamine in mice. Neuropharmacology 61:992–1000. CrossRef Medline

Kawamura Y, Fukaya M, Maejima T, Yoshida T, Miura E, Watanabe M, Ohno-Shosaku T, Kano M (2006) The CB_1 cannabinoid receptor is the major cannabinoid receptor at excitatory presynaptic sites in the hippocampus and cerebellum. J Neurosci 26:2991–3001. CrossRef Medline

Kramer ML, Schulz-Schaeffer WJ (2007) Presynaptic α-synuclein aggregates, not Lewy bodies, cause neurodegeneration in dementia with Lewy bodies. J Neurosci 27:1405–1410. CrossRef Medline

Kuwahara T, Koyama A, Koyama S, Yoshina S, Ren CH, Kato T, Mitani S, Iwatsubo T (2008) A systematic RNAi screen reveals involvement of endocytic pathway in neuronal dysfunction in alpha-synuclein transgenic C. elegans. Hum Mol Genet 17:2997–3009. CrossRef Medline

Larsen KE, Schmitz Y, Troyer MD, Mosharov E, Dietrich P, Quazi AZ, Savalle M, Nemani V, Chaudhry FA, Edwards RH, Stefanis L, Sulzer D (2006) α-Synuclein overexpression in PC12 and chromaffin cells impairs catecholamine release by interfering with a late step in exocytosis. J Neurosci 26:11915–11922. CrossRef Medline

Majewski H, Iannazzo L (1998) Protein kinase C: a physiological mediator of enhanced transmitter output. Prog Neurobiol 55:463–475. CrossRef Medline

Maroteaux L, Campanelli JT, Scheller RH (1988) Synuclein: a neuron-specific protein localized to the nucleus and presynaptic nerve terminal. J Neurosci 8:2804–2815. Medline

Masliah E, Rockenstein E, Veinbergs I, Sagara Y, Mallory M, Hashimoto M, Mucke L (2001) beta-amyloid peptides enhance alpha-synuclein accumulation and neuronal deficits in a transgenic mouse model linking Alzheimer's disease and Parkinson's disease. Proc Natl Acad Sci U S A 98:12245–12250. CrossRef Medline

McFarland MA, Ellis CE, Markey SP, Nussbaum RL (2008) Proteomics analysis identifies phosphorylation-dependent alpha-synuclein protein interactions. Mol Cell Proteomics 7:2123–2137. CrossRef Medline

Miyazaki T, Fukaya M, Shimizu H, Watanabe M (2003) Subtype switching of vesicular glutamate transporters at parallel fibre-Purkinje cell synapses in developing mouse cerebellum. Eur J Neurosci 17:2563–2572. CrossRef Medline

Morgan A, Burgoyne RD, Barclay JW, Craig TJ, Prescott GR, Ciufo LF, Evans GJ, Graham ME (2005) Regulation of exocytosis by protein kinase C. Biochem Soc Trans 33:1341–1344. CrossRef Medline

Morgan JR, Prasad K, Hao W, Augustine GJ, Lafer EM (2000) A conserved clathrin assembly motif essential for synaptic vesicle endocytosis. J Neurosci 20:8667–8676. Medline

Murphy DD, Rueter SM, Trojanowski JQ, Lee VM (2000) Synucleins are developmentally expressed, and α-synuclein regulates the size of the presynaptic vesicular pool in primary hippocampal neurons. J Neurosci 20:3214–3220. Medline

Nagy G, Matti U, Nehring RB, Binz T, Rettig J, Neher E, Sørensen JB (2002) Protein kinase C-dependent phosphorylation of synaptosome-associated protein of 25 kDa at Ser187 potentiates vesicle recruitment. J Neurosci 22:9278–9286. Medline

Nemani VM, Lu W, Berge V, Nakamura K, Onoa B, Lee MK, Chaudhry FA, Nicoll RA, Edwards RH (2010) Increased expression of alpha-synuclein reduces neurotransmitter release by inhibiting synaptic vesicle reclustering after endocytosis. Neuron 65:66–79. CrossRef Medline

Neumann M, Kahle PJ, Giasson BI, Ozmen L, Borroni E, Spooren W, Müller V, Odoy S, Fujiwara H, Hasegawa M, Iwatsubo T, Trojanowski JQ, Kretzschmar HA, Haass C (2002) Misfolded proteinase K-resistant hyperphosphorylated alpha-synuclein in aged transgenic mice with locomotor deterioration and in human alpha-synucleinopathies. J Clin Invest 110:1429–1439. CrossRef Medline

Orimo S, Uchihara T, Nakamura A, Mori F, Kakita A, Wakabayashi K, Takahashi H (2008) Axonal alpha-synuclein aggregates herald centripetal degeneration of cardiac sympathetic nerve in Parkinson's disease. Brain 131:642–650. CrossRef Medline

Pan-Montojo F, Anichtchik O, Dening Y, Knels L, Pursche S, Jung R, Jackson S, Gille G, Spillantini MG, Reichmann H, Funk RH (2010) Progression of Parkinson's disease pathology is reproduced by intragastric administration of rotenone in mice. PLoS One 5:e8762. CrossRef Medline

Saito Y, Kawashima A, Ruberu NN, Fujiwara H, Koyama S, Sawabe M, Arai T, Nagura H, Yamanouchi H, Hasegawa M, Iwatsubo T, Murayama S (2003) Accumulation of phosphorylated alpha-synuclein in aging human brain. J Neuropathol Exp Neurol 62:644–654. Medline

Sakisaka T, Yamamoto Y, Mochida S, Nakamura M, Nishikawa K, Ishizaki H, Okamoto-Tanaka M, Miyoshi J, Fujiyoshi Y, Manabe T, Takai Y (2008) Dual inhibition of SNARE complex formation by tomosyn ensures controlled neurotransmitter release. J Cell Biol 183:323–337. CrossRef Medline

Schulz-Schaeffer WJ (2010) The synaptic pathology of alpha-synuclein aggregation in dementia with Lewy bodies, Parkinson's disease and Parkinson's disease dementia. Acta Neuropathol 120:131–143. CrossRef Medline

Scott DA, Tabarean I, Tang Y, Cartier A, Masliah E, Roy S (2010) A pathologic cascade leading to synaptic dysfunction in α-synuclein-induced neurodegeneration. J Neurosci 30:8083–8095. CrossRef Medline

Sharma M, Burré J, Südhof TC (2011) CSPalpha promotes SNARE-complex assembly by chaperoning SNAP-25 during synaptic activity. Nat Cell Biol 13:30–39. CrossRef Medline

Shimazaki Y, Nishiki T, Omori A, Sekiguchi M, Kamata Y, Kozaki S, Takahashi M (1996) Phosphorylation of 25-kDa synaptosome-associated protein. Possible involvement in protein kinase C-mediated regulation of neurotransmitter release. J Biol Chem 271:14548–14553. CrossRef Medline

Shoji-Kasai Y, Itakura M, Kataoka M, Yamamori S, Takahashi M (2002) Protein kinase C-mediated translocation of secretory vesicles to plasma membrane and enhancement of neurotransmitter release from PC12 cells. Eur J Neurosci 15:1390–1394. CrossRef Medline

Spillantini MG, Goedert M (2000) The alpha-synucleinopathies: Parkinson's disease, dementia with Lewy bodies, and multiple system atrophy. Ann N Y Acad Sci 920:16–27. Medline

Südhof TC (2004) The synaptic vesicle cycle. Annu Rev Neurosci 27:509–547. CrossRef Medline

Tabuchi K, Blundell J, Etherton MR, Hammer RE, Liu X, Powell CM, Südhof TC (2007) A Neuroligin-3 mutation implicated in autism increases inhibitory synaptic transmission in mice. Science 318:71–76. CrossRef Medline

Tapia-González S, Giráldez-Pérez RM, Cuartero MI, Casarejos MJ, Mena MÁ, Wang XF, Sánchez-Capelo A (2011) Dopamine and alpha-synuclein dysfunction in Smad3 null mice. Mol Neurodegener 6:72. CrossRef Medline

Tong J, Wong H, Guttman M, Ang LC, Forno LS, Shimadzu M, Rajput AH, Muenter MD, Kish SJ, Hornykiewicz O, Furukawa Y (2010) Brain alpha-synuclein accumulation in multiple system atrophy, Parkinson's disease and progressive supranuclear palsy: a comparative investigation. Brain 133:172–188. CrossRef Medline

Ubhi K, Low P, Masliah E (2011) Multiple system atrophy: a clinical and neuropathological perspective. Trends Neurosci 34:581–590. CrossRef Medline

Wickens JR, Arbuthnott GW (2005) Structural and functional interactions in the striatum at the receptor level. In: Dopamine, Handbook of Chemical Neuroanatomy, Vol 21 (Dunnett SB, Bentivoglio M, Björklund A, Hökfelt T, eds), pp 199–236. Amsterdam: Elsevier.

Yamamori S, Itakura M, Sugaya D, Katsumata O, Sakagami H, Takahashi M (2011) Differential expression of SNAP-25 family proteins in the mouse brain. J Comp Neurol 519:916–932. CrossRef Medline

Yasuda T, Hayakawa H, Nihira T, Ren YR, Nakata Y, Nagai M, Hattori N, Miyake K, Takada M, Shimada T, Mizuno Y, Mochizuki H (2011) Parkin-mediated protection of dopaminergic neurons in a chronic MPTP-minipump mouse model of Parkinson disease. J Neuropathol Exp Neurol 70:686–697. CrossRef Medline

Yasuda T, Nakata Y, Mochizuki H (2012) α-Synuclein and neuronal cell death. Mol Neurobiol. Advance online publication. Retrieved November 8, 2012. doi:10.1007/s12035-012-8327-0. CrossRef

Yoshida M (2007) Multiple system atrophy: α-synuclein and neuronal degeneration. Neuropathology 27:484–493. CrossRef Medline

Imaizumi *et al. Molecular Brain* 2012, **5**:35
http://www.molecularbrain.com/content/5/1/35

Molecular Brain

RESEARCH Open Access

Mitochondrial dysfunction associated with increased oxidative stress and α-synuclein accumulation in PARK2 iPSC-derived neurons and postmortem brain tissue

Yoichi Imaizumi[1], Yohei Okada[1,2], Wado Akamatsu[1], Masato Koike[3], Naoko Kuzumaki[1], Hideki Hayakawa[4], Tomoko Nihira[4], Tetsuro Kobayashi[5], Manabu Ohyama[5], Shigeto Sato[6], Masashi Takanashi[6], Manabu Funayama[6,7], Akiyoshi Hirayama[8], Tomoyoshi Soga[8], Takako Hishiki[9], Makoto Suematsu[9], Takuya Yagi[10], Daisuke Ito[10], Arifumi Kosakai[10], Kozo Hayashi[11], Masanobu Shouji[11], Atsushi Nakanishi[11], Norihiro Suzuki[10], Yoshikuni Mizuno[12], Noboru Mizushima[13], Masayuki Amagai[5], Yasuo Uchiyama[3], Hideki Mochizuki[4,14], Nobutaka Hattori[6,7] and Hideyuki Okano[1*]

Abstract

Background: Parkinson's disease (PD) is a neurodegenerative disease characterized by selective degeneration of dopaminergic neurons in the substantia nigra (SN). The familial form of PD, PARK2, is caused by mutations in the *parkin* gene. *parkin*-knockout mouse models show some abnormalities, but they do not fully recapitulate the pathophysiology of human PARK2.

Results: Here, we generated induced pluripotent stem cells (iPSCs) from two PARK2 patients. PARK2 iPSC-derived neurons showed increased oxidative stress and enhanced activity of the nuclear factor erythroid 2-related factor 2 (Nrf2) pathway. iPSC-derived neurons, but not fibroblasts or iPSCs, exhibited abnormal mitochondrial morphology and impaired mitochondrial homeostasis. Although PARK2 patients rarely exhibit Lewy body (LB) formation with an accumulation of α-synuclein, α-synuclein accumulation was observed in the postmortem brain of one of the donor patients. This accumulation was also seen in the iPSC-derived neurons in the same patient.

Conclusions: Thus, pathogenic changes in the brain of a PARK2 patient were recapitulated using iPSC technology. These novel findings reveal mechanistic insights into the onset of PARK2 and identify novel targets for drug screening and potential modified therapies for PD.

Keywords: Induced pluripotent stem cells, Parkinson's disease, Parkin, Oxidative stress, Mitochondria, α-synuclein

Background

Parkin is a causative gene of autosomal recessive juvenile Parkinson's disease (PARK2). It encodes a component of an E3 ubiquitin ligase involved in mitochondrial homeostasis [1-5]. *Parkin* deficiency is thought to result in aberrant ubiquitination and compromised mitochondrial integrity, leading to neuronal dysfunction and degeneration. Several PARK2 mouse models exist, but they do not replicate all of the pathogenic changes seen in human PARK2 neurons; thus, these models do not fully account for the molecular mechanisms of PD [6-9]. A recent report demonstrated that there is a defect in dopamine (DA) utilization in PARK2 induced pluripotent stem cell (iPSC)-derived neurons [10]. However, it is not known whether neuronal homeostasis is disrupted in PARK2 patients. Furthermore, studies have yet to demonstrate whether the phenotype of PD-specific iPSC-derived neurons recapitulates the *in vivo* phenotype of the corresponding cell donor. To address these questions, we generated iPSCs from two PARK2 patients

* Correspondence: hidokano@a2.keio.jp
[1]Department of Physiology, Keio University School of Medicine, 35 Shinanomachi, Shinjuku-ku, Tokyo 160-8582, Japan
Full list of author information is available at the end of the article

(PA and PB) [11]. In PARK2 iPSC-derived neurons, but not PARK2 fibroblasts or iPSCs, abnormal mitochondrial morphology and aberrant tubulovesicular structures adjacent to the Golgi were observed, as was increased oxidative stress. Although α-synuclein accumulation and Lewy body (LB) formation are very rare in PARK2 patients [1,12,13], we observed pathological changes and prominent LB formation, including the accumulation of α-synuclein, in postmortem brain tissue from one of the donor patients (PA). However, we obtained autopsied brain tissue from the father of donor PB, who carried the same *parkin* deletion as PB, and observed no evidence of LB formation or α-synuclein-positive cells. Consistent with these observations in postmortem brain tissue, increased α-synuclein accumulation was clearly observed in PA iPSC-derived neurons *in vitro,* but not in PB iPCS-derived neurons. These results are the first demonstration of pathogenic changes in the brain of a PARK2 patient that were recapitulated using iPSC technology. Our findings also provide mechanistic insights into PARK2 pathophysiology.

Results & discussion

Generation of PARK2 iPSCs

iPSCs were generated from dermal fibroblasts isolated from two PARK2 patients carrying *parkin* mutations and two control subjects using retroviruses carrying *Oct4, Sox2, Klf4,* and *c-Myc* to reprogram the cells as previously described [14,15]. The PARK2 patients were a 71-year-old female (PA) with a homozygous deletion of *parkin* exons 2–4 and a 50-year-old male (PB) with a homozygous deletion of exons 6 and 7 (Table 1 and Additional file 1A and B). Patient PA died 1 year after enrollment in the study at the age of 72. A previously-established human iPSC clone from control subject A, 201B7 (B7), was also used [15]. In addition, the following human embryonic stem cell (hESC)-like iPSC clones were selected for detailed analysis: three controls (B7 and YA9 from control A, and WD39 from control B), three from patient PA (PA1, PA9 and PA22), and four from patient PB (PB1, PB2, PB18 and PB20) (Figure 1A and Additional file 2A and B).

The PARK2 iPSCs expressed pluripotent hESC markers (Figure 1A and Additional file 2A-C) and formed teratomas containing all three germ layers (Additional file 2D).

Table 1 PA and PB patient information

	PA patient	PB patient
Race	Japanese	Japanese
Age	72 y/o	50 y/o
Sex	Female	Male
Age of onset	62 y/o	28 y/o
Mutation of *parkin*	Exon 2–4 homozygous deletions	Exon 6, 7 homozygous deletions

All of the retroviral transgenes were silenced in each clone (Additional file 2E). The iPSCs derived from PA and PB retained the corresponding homozygous *parkin* deletions and exhibited genomic stability (Figure 1B-D; Additional file 3A and B; and Table 1). All of the clones differentiated into neurons, including tyrosine hydroxylase (TH)-positive neurons, through a process of embryoid body and neurosphere formation (Figure 1A). Thus, all of the lines were successfully reprogrammed into a pluripotent state and were suitable for further analysis.

Increased oxidative stress accompanied by activation of the Nrf2 pathway in PARK2 iPSC-derived neurons

Because increased levels of oxidative stress have been documented in other PD models [7,10,16,17], we examined oxidative metabolism in the iPSC clones by measuring the cellular levels of reduced glutathione (GSH). GSH reacts with reactive oxygen species (ROS) and is catalyzed by glutathione S-transferase[18]. Consistent with previous results from patient-derived cells [16], the levels of GSH in PARK2 iPSC-derived neurospheres were significantly lower than those in control iPSC-derived neurospheres (Figure 2A). We also examined ROS production using 2', 7'-dichlorodihydrofluorescin (DCF) fluorescence to measure the levels of intracellular oxidants. The DCF fluorescence intensity in the PARK2 iPSC-derived neurons was significantly higher than that in control iPSC-derived neurons (Figure 2B and C), which indicated an increased level of oxidative stress. A recent study showed that, in PARK2 iPSC-derived neurons, monoamine oxidase (MAO)-A and -B levels and oxidative stress levels are increased, as is spontaneous DA release [10]. Here, we found no significant differences in MAO-A and -B expression levels between PARK2 and control neurons (Additional file 4A and B).

The Nrf2 pathway plays a cytoprotective role under conditions of ROS accumulation. Recent studies show that activation of the Nrf2 pathway reduces oxidative stress and provides partial protection from MPTP-mediated neurotoxicity[19]. Elevated Nrf2 expression was observed in the postmortem brain of a PD patient [20]. These data suggest a putative link between the Nrf2 pathway and PD, and prompted a closer investigation of this signaling pathway in control and PARK2 iPSC-derived neurons [19-21]. The expression of Nrf2 pathway proteins, such as Nrf2 and NADH quinone oxidoreductase (NQO1), was significantly increased in PARK2 iPSC-derived neurons (Figure 2D and E). These data are in line with previous reports [19-21], and suggest that the Nrf2 cytoprotective pathway may be activated in PARK2 iPSC-derived neurons to prevent further damage from oxidative stress. Taken together, these data demonstrated an increased level of

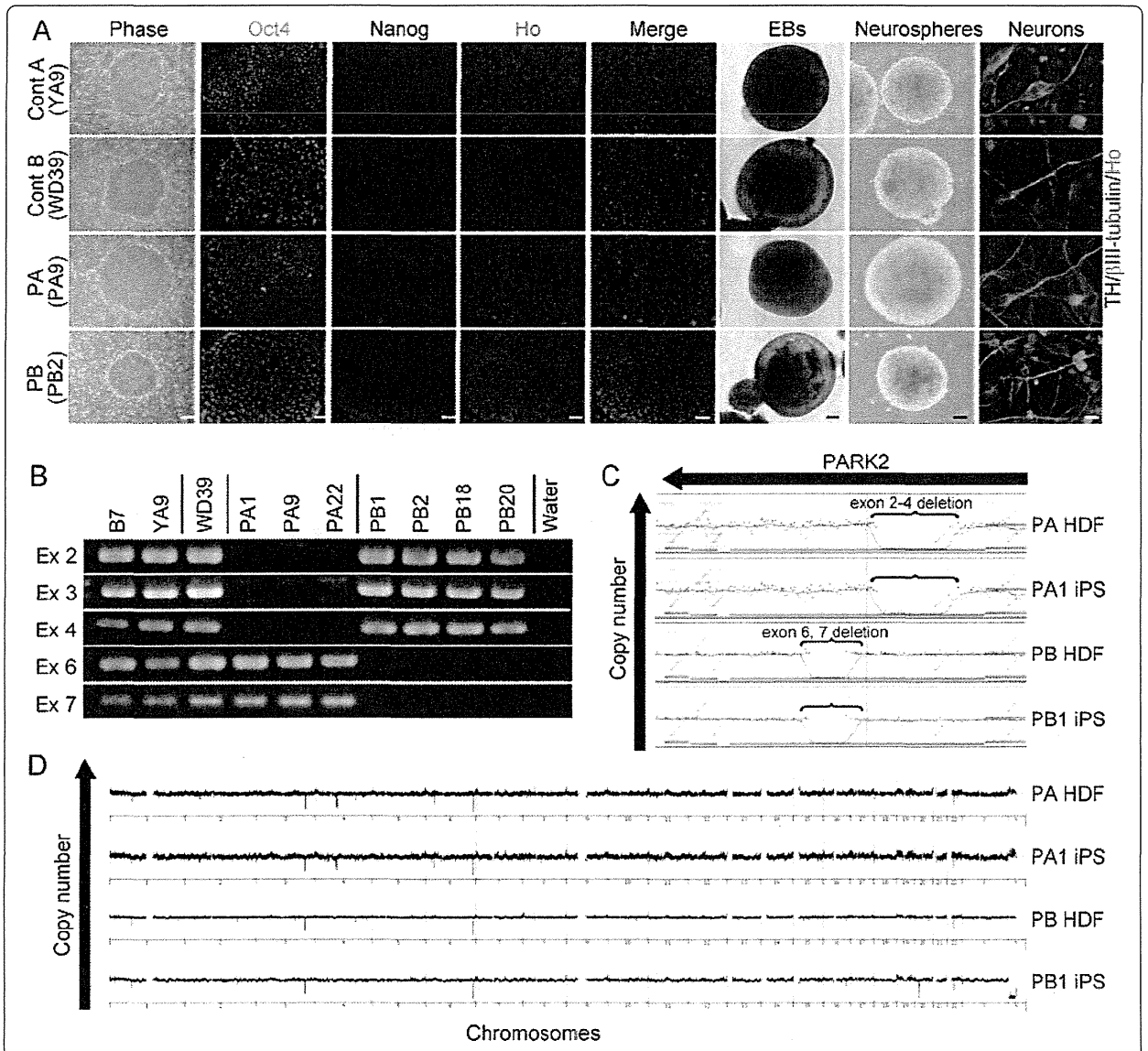

Figure 1 Generation of PARK2 iPSCs. (**A**) iPSCs derived from control and PARK2 subjects, embryoid bodies (EBs), neurospheres (NSs), and neurons. *Left three rows:* iPSCs from Control A (YA9), Control B (WD39), PA (PA9), and PB (PB2) were immunopositive for the pluripotency markers Oct4 (green) and Nanog (red). *Right three rows:* Differentiation of iPSCs into tyrosine hydroxylase (TH)-positive (red) neurons via EB and NS formation. Scale bars: Phase contrast, 400 μm; Nanog and Oct4 immunostaining, 100 μm; EBs, 25 μm; NSs, 50 μm; neurons, 10 μm. (**B**) Deletion of exons 2–4 in clones PA1, 9 and 22; and of exons 6 and 7 in clones PB1, 2, 18, and 20 was confirmed. (**C**) Exons 2–4 were deleted in human dermal fibroblasts (HDFs) from PA and in PA1 iPSC lines. Exons 6 and 7 were deleted in HDFs from PB and PB1 iPSC lines. (**D**) Copy number profiles of whole chromosomes in PARK2 HDFs and iPSCs were assessed by comparative genomic hybridization (CGH) microarray analysis; there was no evidence that genomic aberrations were introduced during the process of establishing PARK2 iPSCs.

oxidative stress accompanied by activation of the Nrf2 pathway in PARK2 neurons.

Abnormal mitochondrial morphology and impaired mitochondrial turnover in PARK2 iPSC-derived neurons

Increased oxidative stress (which affects anti-oxidant defense systems) and mitochondrial dysfunction are implicated in the pathogenesis of PD [1,13,21-23]. Furthermore, ROS accumulation causes both oxidative damage and mitochondrial dysfunction in the substantia nigra (SN) of *parkin*-deficient mice [7]. However, the exact mechanism of mitochondrial pathogenesis associated with PARK2 is controversial. For example, while *Drosophila parkin* mutants show abnormal mitochondrial morphology, *parkin*-knockout mice do not [7,24]. In addition, while a greater degree of mitochondrial branching is observed in

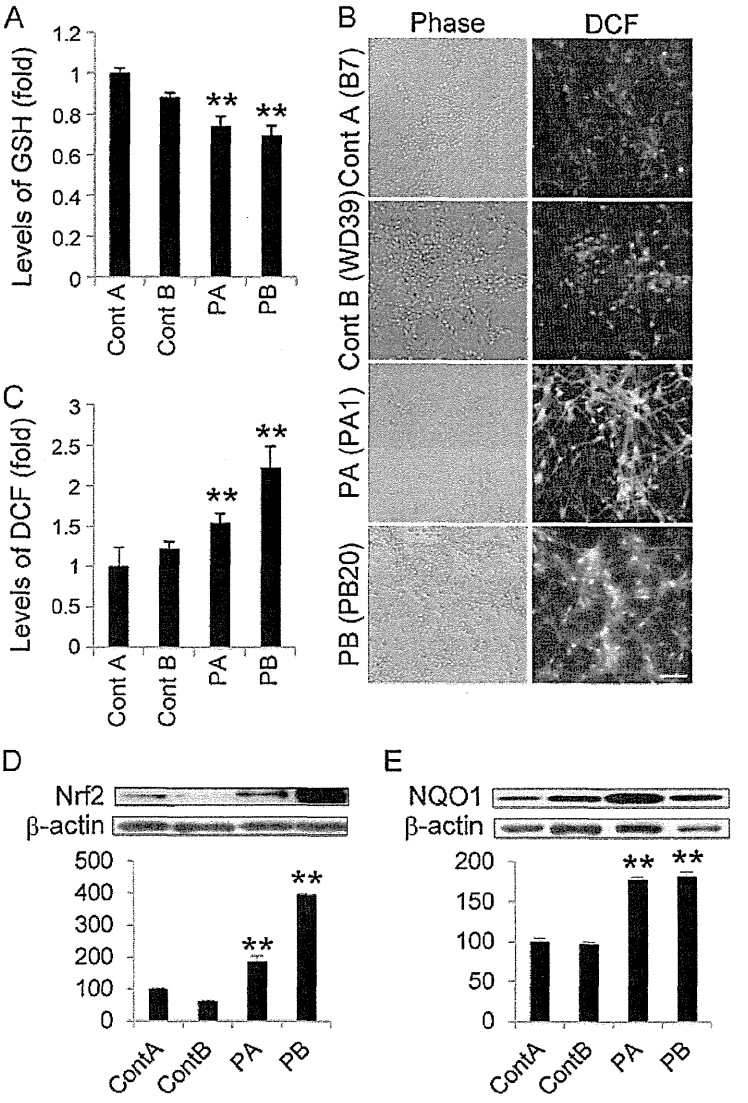

Figure 2 Increased oxidative stress accompanied by activation of the Nrf2 pathway in PARK2 iPSC-derived neurons. (**A**) GSH levels were significantly reduced in PARK2 (PA1, 9 and 22, and PB2, 18 and 20) iPSC-derived neurospheres compared with those in control A (YA9) and B (WD39) neurospheres. (**B, C**) DCF fluorescence intensity in PARK2 (PA1, 9 and 22, and PB2 and 20) iPSC-derived neurons was significantly higher than that in control A (B7) and B (WD39) neurons. (**D, E**) Immunoblot analysis of Nrf2 and NQO1 levels in iPSC-derived neurons from PA and PB. Expression of Nrf2 and NQO1 in PARK2 (PA9 and PB2) iPSC-derived neurons was significantly higher than that in control A (YA9) and B (WD39) neurons. Relative protein abundance was normalized to β-actin. ** indicates $P < 0.01$ (Mann–Whitney *U*-test). Data represent the mean and SEM of at least three experiments for each group.

fibroblasts derived from PARK2 patients, the detailed morphology of the mitochondria in these cells has not been characterized [25]. To investigate these mitochondrial abnormalities in more depth, we performed a detailed morphological analysis of mitochondria in PARK2 iPSC-derived neurons using electron microscopy. Mitochondria in PARK2 neurons from both patients showed a highly electron-dense matrix and swollen mitochondrial cristae within the inner mitochondrial membrane (IMM) (Figure 3A, black arrowheads). The perikaryal volume density of the abnormal mitochondria was significantly increased in PA and PB iPSC-derived neurons relative to control clones (Figure 3B). Furthermore, the density of normal mitochondria decreased (Figure 3B). Importantly, both abnormal and normal mitochondria were observed in PARK2 neurons (Figure 3A, white arrowheads). Abnormal mitochondria were observed in 87.8% of iPSC-derived neurons from PA, and 79.5% of iPSC-derived neurons from PB. These data indicated that abnormal mitochondrial morphology was a feature of most PARK2 iPSC-derived

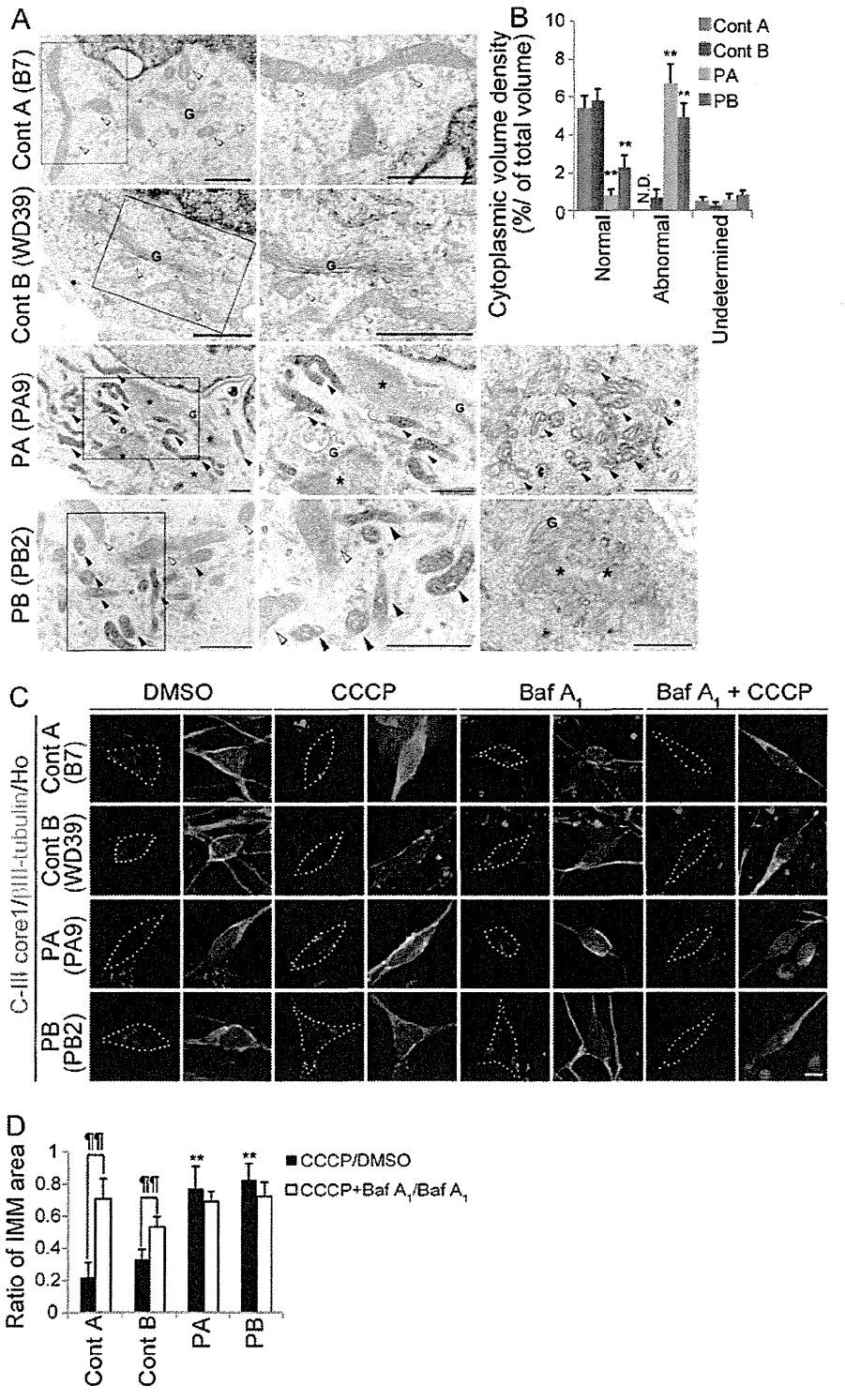

Figure 3 (See legend on next page.)

(See figure on previous page.)
Figure 3 Dysregulation of mitochondrial homeostasis in PARK2 iPSC-derived neurons. (**A**) Electron micrographs of control A (B7), control B (WD39) and PARK2 (PA9 and PB2) iPSC-derived neurons. Boxed areas are shown in the enlarged images to the right. Control mitochondria showed a characteristically long, cylindrical profile with well-organized cristae, and the electron density of the matrix was relatively low (white arrowheads). By contrast, increased electron density of the matrix was evident in PARK2 mitochondria (black arrowheads), and the cristae often appeared swollen. As shown in PB2, some of the neurons contained both morphologically intact (white arrowheads) and abnormal (black arrowheads) mitochondria. Furthermore, abnormal tubulovesicular structures (asterisks) were observed adjacent to the Golgi cisternae (G). (**B**) The relative perikaryal volume of the abnormal mitochondria was significantly increased, and that of the normal mitochondria was decreased, in PARK2 neurons compared with control neurons. (**C**) Double labeling for the IMM marker, ComplexIII corel (CIII-Core I; magenta) and βIII-tubulin (green) of control A (B7), control B (WD39) and PARK2 (PA9 and PB2) iPSC-derived neurons. The volume of the IMM area was reduced in control neurons treated with CCCP, but not in PARK2 neurons treated with CCCP. Administration of Baf A_1 rescued the CCCP-induced phenotype in control neurons. (**D**) The CCCP/DMSO ratio in control A (B7 and YA9) and B (WD39) neurons was reduced after CCCP treatment. This reduction was not observed in PARK2 (PA1, 9 and 22, and PB2 and 20) iPSC-derived neurons (black bars indicate CCCP/DMSO ratio; white bars indicate Baf A_1+CCCP/Baf A_1 ratio). ** indicates $P < 0.01$ compared with the control; ¶¶ indicates $P < 0.01$ when comparing the black and white bars (Mann–Whitney *U*-test). At least three experiments were performed for each group, with 5–36 cells quantified per experiment. Scale bars: a, 1 μm; c, 10 μm. Error bars represent the SEM. N.D., not detected.

neurons from these patients. In addition, abnormal tubulovesicular structures were observed adjacent to the Golgi cisternae in PARK2 iPSC-derived neurons (Figure 3A). These abnormal mitochondrial and tubulovesicular structures were not observed in PARK2 fibroblasts or in undifferentiated iPSCs (Additional file 5A and B). These histological abnormalities represent novel PARK2-related neuronal pathologies.

PARKIN is involved in the mitochondrial fission/fusion system and is recruited to depolarized mitochondria to promote mitophagy [5,26-29]. In iPSC-derived neurons containing a mutation in PINK1 (a protein kinase upstream of PARKIN), PARKIN is not recruited appropriately to mitochondria [30]. We hypothesized that PARKIN-deficient human neurons would show aberrant removal of depolarized mitochondria. To examine the turnover of damaged mitochondria, we treated iPSC-derived neurons with carbonyl cyanide m-chlorophenyl hydrazine (CCCP), which triggers the loss of mitochondrial membrane potential and results in the removal of damaged mitochondria. The intensity of TMRE, a mitochondrial membrane potential-dependent dye, clearly decreased in both control and PARK2 iPSC-derived neurons treated with CCCP, which indicated a reduced mitochondrial membrane potential in both sets of neurons (Additional file 6). To determine the extent to which the damaged mitochondria were eliminated, we measured the area of the IMM after CCCP treatment. Compared with untreated cells, there was a dramatic loss of IMM area in the treated control neurons, but not in the treated PARK2 neurons (Figure 3C, left four columns; Figure 3D, black bars). To assess whether lysosomes were involved in the CCCP-induced elimination of mitochondria, we treated cells with Bafilomycin (Baf) A_1, an inhibitor of the vacuolar type H(+)-ATPase. Baf A_1 attenuated the CCCP-dependent reduction in the IMM area in control neurons (Figure 3C, right four columns; Figure 3D, white bars). To confirm that the abnormal turnover of damaged mitochondria was characteristic of neuronal cells, PARK2 fibroblasts and undifferentiated iPSCs were treated with CCCP. CCCP-treated PARK2 fibroblasts and undifferentiated iPSCs exhibited the same mitochondrial dynamics as CCCP-treated control cells (Additional file 5C-E). Together, these data indicated aberrant degradation of mitochondria damaged by CCCP treatment in PARK2 iPSC-derived neurons.

These results support a recently proposed working model for PD, in which damaged mitochondria accumulate due to a disruption in PARKIN-mediated mitochondrial quality control [28]. The electron microscopy data, which showed a mixture of abnormal and normal mitochondria, indicated that PARKIN-mediated mitochondrial quality control is compromised, even in young PARK2 iPSC-derived neurons. In these cells, residual normal mitochondria may have compensated for the damaged ones. Thus, while our findings suggest that the PARKIN-dependent mechanisms that regulate mitochondrial homeostasis are disrupted in PARK2 cells, further detailed analyses are required to fully understand the mechanism underlying this disruption and the implications for PD.

Patient-specific accumulation of α-synuclein in PARK2 iPSC-derived neurons and its correlation with LB formation

LBs are pathological neuronal inclusions composed principally of α-synuclein. They are typically associated with PD and certain forms of dementia [1,13,31]. Although LBs are generally thought to be absent from PARK2 patients [1,13,31], rare cases of LB formation in the brains of PARK2 patients have been reported recently [12,32,33]. The PARKIN protein co-localizes with LBs in some patients with sporadic PD [34], and a functional interaction between PARKIN and α-synuclein is indicated by both *in vitro* and *in vivo* findings [35-37]. These results suggest that PARKIN-pathway may contribute to LB formation in PD patients.

We were able to conduct a histopathological analysis of postmortem brain tissue from patient PA. Hematoxylin and eosin staining of the SN revealed low levels of brown-black

melanin pigment compared with healthy SN tissue (Figure 4A and A'). Surprisingly, LBs accumulated in the SN and other areas of the brain in patient PA (Figure 4B and Table 2). Furthermore, α-synuclein and pα-synuclein immunoreactive puncta and neurites were observed in the areas where LBs were present (Figure 4B). TH/pα-synuclein double-positive neurons were also detected in the SN (Figure 4C). Of note, α-synuclein-positive/TH-negative or pα-synuclein-positive/TH-negative neurons in the SN and other areas of the brain tissue from patient PA's brain were observed (Table 2). These data suggested that α-synuclein accumulated not only in TH+ neurons, but also in other types of neurons. Postmortem tissue from the brain of the father of patient PB was also examined. The father carried a homozygous deletion of exons 6 and 7 of the *parkin* gene (Figure 1B, Additional file 1B and 7A), similar to patient PB. There was no evidence of LBs or α-synuclein-positive neurons in the autopsied brain tissue of the father (Figure 4D). Thus, since the genetic background of patient PB and his father are likely to be very close (Additional file 1B and 7A), these results are probably reflective of a specific phenotype of patient PB, which was different from that in patient PA (Figure 4A-D).

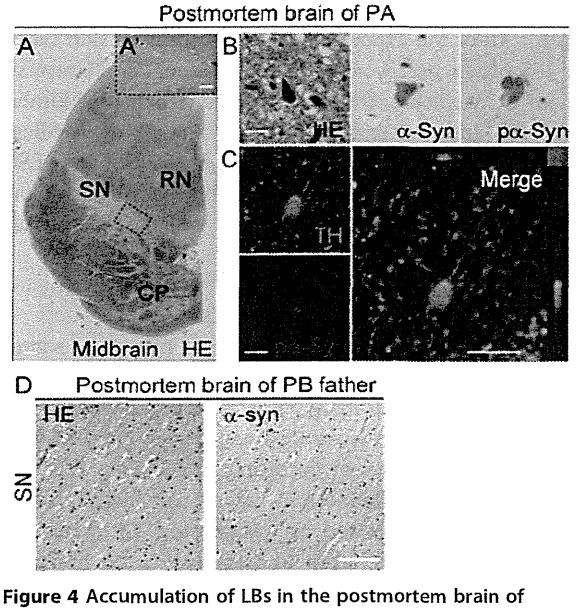

Figure 4 Accumulation of LBs in the postmortem brain of patient PA. (**A–C**) Immunohistochemical staining of postmortem brain tissue from patient PA. (**A**) Low magnification image of a midbrain section stained with hematoxylin and eosin (H&E). (**A'**) High magnification image of the boxed area. Melanin levels were reduced in most of the substantia nigra (SN). (**B**) (Left) High magnification image of a midbrain section stained with H&E showing the presence of Lewy bodies (LBs) in the SN. (Middle and Right) α-synuclein-positive and pα-synuclein-positive cells in the SN. (**C**) Confocal microscopy image of a TH (green) and pα-synuclein (red) double-positive SN neuron and a projected merged image: pα-synuclein accumulated in the TH-positive neuron. (**D**) Melanin levels were reduced in most of the SN. No LBs or α-synuclein-positive neurons were observed in postmortem brain tissue from the father of patient PB. Scale bars: A, 1000 μm; A', 350 μm; B, C, 50 μm; D, 100 μm.

To determine whether iPSC-derived neurons recapitulated the *in vivo* phenotypes of the corresponding cell donors, we next examined α-synuclein accumulation in PARK2 iPSC-derived neurons. To rule out the possibility that α-synuclein expression in undifferentiated PARK2 iPSCs was increased by multiplication of the *SNCA* gene, genomic aberrations acquired during the process of iPSC establishment, or by repeated passage of the cells, the *SNCA* gene copy number in iPSCs was quantified by genomic qPCR. A comparison with control iPSCs showed that iPSCs from both PA and PB carried the normal number of *SNCA* gene copies (Additional file 8A). Moreover, immunostaining for α-synuclein did not reveal any increase or decrease in α-synuclein protein levels in PARK2 iPSCs (Additional file 8B). As a control for LB formation, we generated iPSC-derived neurons from a 106-year-old woman (designated Cent1-8), since previous work suggested that aging is a predisposing factor for LB formation in PD patients [31,38]. Since α-synuclein was also expressed in non-neural cells, triple labeling for α-synuclein, βIII-tubulin, and TH was performed to ensure that only neurons were examined (Figure 5A, asterisks). The proportion of α-synuclein-positive iPSC-derived neurons that were also positive for βIII-tubulin from PB was similar to that in the controls (including Cent1-8); however, the proportion was significantly higher in PA. These results were consistent with the *in vivo* phenotypes of the cell donors based on analysis of postmortem brain tissue (1629, 357, 805, 3747, and 4330 iPSC-derived βIII-tubulin+ neurons in control A, control B, Cent1-8, PA and PB respectively; Figure 5A-C, arrows and arrowheads). Thus, the increase in α-synuclein expression levels seen in PARK2 iPSC-derived neurons

Table 2 LB type pathology in PA patient's postmortem brain

Brain area		LB type pathology
Brainstem lesion	IX-X	+++
	LC	+++
	SN	++
Basal forebrain/Limbic	nbM	++
	Amy	++
	Ent	+
	Cing	+
Neocortical	T	-
	F	-
	P	-

IX-X, motor cranial nerves IX-X; *LC*, Locus Coeruleus; *SN*, Substantia Nigra; *nbM*, nucleus basal of Meynert; Amy, Amygdala; Ent, Entorhinal cortex; T, Temporal lobe; F, Frontal lobe; P, Parietal lobe.

cannot be attributed solely to the effects of aging, but associated with the disease phenotype.

The obvious LB-formation was observed in the postmortem brain of PA patient, who showed a late onset at 61 years, corresponding to the enhanced α-synuclein accumulation in the iPSC-derived neurons from the same patient. Thus, it is likely that early-stage LB formation was recapitulated *in vitro* in iPSC-derived neurons. Furthermore, the present findings are consistent with recent work by several groups, which suggest that the age of onset of PARK2 in patients with LB formation (41 on average) is later than in patients without LB formation (below 40) [12,32,33]. The earlier onset in patient PB (at 28 years) than in PA (at 61 years) would be consistent with the finding of lower α-synuclein accumulation in PB iPSC-derived neurons compared with PA iPSC-derived neurons. On the other hand, and in contrast to the observations of brain tissue from PA, analysis of brain tissue from the father of patient PB, in whom the onset of PD was 39 years of age, revealed no evidence of LB formation (Figure 4D). Importantly, PA iPSC-derived neurons showed significantly more α-synuclein accumulation than PB iPSC-derived neurons (Figure 5A and C). These results suggest that the extent of α-synuclein accumulation is an important factor in LB formation. Then, how can we explain the difference of α-synuclein accumulation between PA and PB patients-derived neuronal cells? It is possible that PA is a rare example of PARK2 complicated by sporadic PD. Although both PA and PB iPSCs showed a normal *SNCA* gene copy number, it is possible that PA-derived cells acquired an unknown gene mutation relating to LB formation. Thus, we cannot rule out the possibility that other factors may affect LB formation in PARK2 patients. Further analyses will be required to identify these putative factors. Although iPSC clones from sporadic and familial PD patients were recently established [17,30,39-42], this report is the first to demonstrate that the phenotype of PD-specific iPSC-derived neurons replicates the *in vivo* phenotype seen in postmortem brain tissue from the corresponding cell donor.

Conclusions

In summary, dysfunctional neuronal homeostasis (characterized by increased oxidative stress and activation of the Nrf2 pathway), impaired mitochondrial function, and increased α-synuclein accumulation were observed in PARK2 iPSC-derived neurons. These results indicate that PARK2-associated phenotypes may appear soon after, or possibly even before, the onset of PARK2. Detailed analyses of PARK2 iPSC-derived neurons, particularly mature neurons, to determine the time course of LB accumulation and synaptic dysfunction will be of great interest. Such analyses will further our understanding of the pathogenesis of PARK2 as well as sporadic PD. The ultimate goal is the development and application of novel preventative therapies for PD.

Materials & methods

Isolation of human skin fibroblasts and generation of iPSCs

For control A, human dermal fibroblasts (HDFs) from the facial dermis of a 36-year-old Caucasian female (Cell Applications Inc.) were used to establish iPSCs (201B7; Passage 20–29, YA9; Passage 15–24). The 201B7 iPSCs were kindly provided by Dr. Yamanaka [15]. A skin-punch biopsy from a healthy 16-year-old Japanese female obtained after written informed consent (Keio University School of Medicine) was used to generate the control B iPSCs (WD39; Passage 8–17). PA iPSCs (PA1, 9, and 22; Passage 10–19) and PB iPSCs (PB1, 2, 18, and 20; Passage 8–17) were generated from a 71-year-old Japanese female patient and a 50-year-old Japanese male patient, respectively, using the same methods used to generate control B iPSCs. The maintenance of HDFs, lentiviral production, retroviral production, infection, stem cell culture and characterization, and teratoma formation were performed as described previously [14,15]. All of the experimental procedures for skin biopsy and iPS production were approved by the Keio University School of Medicine Ethics committee (Approval Number: 20-16-18) and Juntendo University School of Medicine Ethics committee (Approval Number: 2012068). hESCs (KhES-1; Passage 29–38 (kindly provided by Dr. Norio Nakatsuji) were cultured on feeder cells in iPS culture media [43].

In vitro differentiation of human iPSCs

Neural differentiation of iPSCs was performed as previously described [44] with slight modifications (Okada et al., manuscript in preparation). Briefly, iPSC colonies were detached from feeder layers and cultured in suspension as EBs for about 30 days in bacteriological dishes. EBs were then enzymatically dissociated into single cells and the dissociated cells cultured in suspension in serum-free media (MHM) [44] for 10 to 14 days to allow the formation of neurospheres. Neurospheres were passaged repeatedly by dissociation into single cells followed by culture in the same manner. Typically, neurospheres between passages 3 and 8 were used for analysis. For terminal differentiation, dissociated or undissociated neurospheres were allowed to adhere to poly-L-ornithine- and fibronectin-coated coverslips and cultured for 10 days.

Immunocytochemical analysis of iPSCs and neurons

For immunocytochemical analysis, cells were fixed with phosphate buffered saline (PBS) containing 4% paraformaldehyde (PFA) for 30 min at room temperature (RT). The cells were analyzed by immunofluorescence staining using antibodies to the following proteins: β-III-tubulin (1:1000,

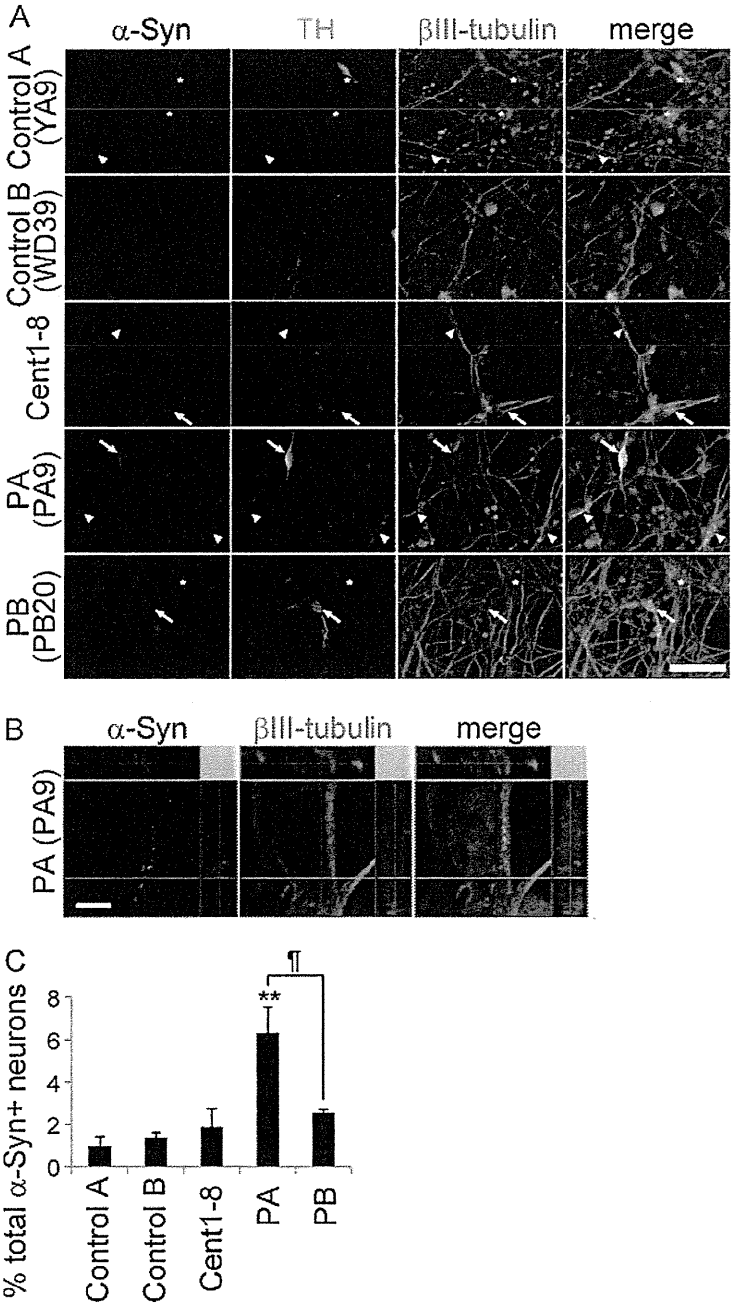

Figure 5 α-synuclein accumulation in PARK2 iPSC-derived neurons. (**A**–**C**) Triple labeling for α-synuclein (red), tyrosine hydroxylase (TH; cyan), and βIII-tubulin (green) along with Hoechst (blue) staining of control A (B7), control B (WD39), Cent1-8, and PARK2 (PA9 and PB20) iPSC-derived neurons. (**A**) Arrows indicate α-synuclein+/TH+/βIII-tubulin+ neurons; arrowheads indicate α-synuclein+/TH-/βIII-tubulin+ neurons. Note the presence of α-synuclein+/TH-/βIII-tubulin- non-neural cells (asterisks). (**B**) High magnification confocal projection image of an α-synuclein (magenta)/βIII-tubulin (green) double-positive PA9 iPSC-derived neuron. (**C**) The proportion of α-synuclein+/βIII-tubulin+ neurons relative to βIII-tubulin-positive neurons was significantly higher in PA (PA1, 9 and 22) iPSC-derived neurons than in control A (B7 and YA9), control B (WD39) and Cent1-8 iPSC-derived neurons. Scale bars: A, 50 μm; C, 5 μm. ** indicates $P < 0.01$; * and ¶ indicate $P < 0.05$ (Mann–Whitney *U*-test). Data represent the mean and SEM of at least three experiments for each group.